

Supporting Information for

**Geometry-dependent valence tautomerism, magnetism, and electrical conductivity
in 1D iron–tetraoxolene chains**

Ashlyn A. Kamin,¹ Ian P. Moseley,² Jeewhan Oh,³ EJ Brannan,¹ Paige M. Gannon,¹ Werner Kaminsky,² Joe M. Zadrozny,² Dianne J. Xiao.^{1,*}

¹Department of Chemistry, University of Washington, Seattle, Washington 98195, United States

²Department of Chemistry, Colorado State University, Fort Collins, Colorado 80523, United States

³Department of Chemistry and Chemical Biology, Harvard University, Cambridge, Massachusetts 02138, United States

*Correspondence to: djxiao@uw.edu

Table of Contents

1.	General Materials and Methods:	2
2.	Synthetic Procedures:	3
3.	Electrochemical Characterization:	8
4.	Dc Magnetic Measurements and Analyses:	9
5.	Ac Magnetic Measurements and Analyses:	11
6.	Single Crystal X-ray Diffraction:	12
7.	Supplementary Tables:	14
8.	Supplementary Figures:	18
9.	Supplementary Crystallographic Data:	35
10.	References:	40

1. General Materials and Methods:

Reactions were performed using standard Schlenk or glovebox techniques under a nitrogen atmosphere unless otherwise specified. Reactions involving hydrated metal salts were performed in a water-containing glovebox, and products were transferred to a water-free glovebox for washing. Reagents and solvents were purchased from commercial vendors (Millipore Sigma, TCI America, Alfa Aesar, Fisher Scientific, Oakwood Chemical, Combi-Blocks) and used without further purification. Deuterated solvents (CDCl_3 , $\text{DMSO-}d_6$, MeOD) were purchased from Cambridge Isotope Laboratories.

NMR spectra were acquired using Bruker AV300, AV301, DRX499, or AV500 spectrometers. All ^1H and ^{13}C NMR spectra were referenced to residual deuterated solvent peaks.

ESI-MS data was collected on a Bruker Esquire Ion Trap in positive ion mode.

High-resolution C, H, N, Br combustion analysis was conducted by Atlantic Microlabs Inc.

Attenuated total reflectance infrared (ATR-IR) spectra were collected on a Perkin Elmer Frontier FT-IR/FIR instrument equipped with a diamond ATR accessory.

Diffuse reflectance UV-vis-NIR spectra were collected on a Shimadzu UV-3600i Plus spectrophotometer equipped with a Harrick Scientific Praying Mantis diffuse reflectance attachment. Samples were diluted with BaSO_4 , ground with a spatula, and analyzed in air immediately following removal from the glovebox. The Kubelka-Munk transformation was performed to convert the spectra from raw reflectance data using the formula $F(R) = (1 - R)^2/2R$, where R is the reflectance and F(R) is the transformed data.

Powder X-ray diffraction (PXRD) data were collected on a Bruker D2 PHASER benchtop diffractometer equipped with a LINXEYE XE-T detector. Dry samples were ground with a spatula and analyzed as powders on a monocrystalline Si substrate.

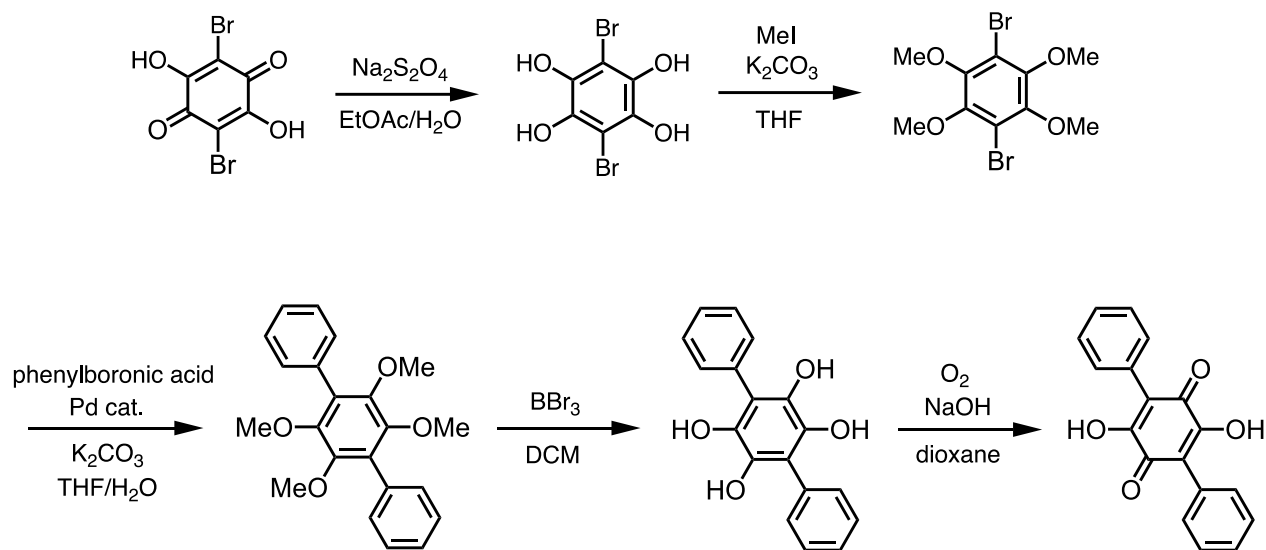
Zero-field ^{57}Fe Mössbauer spectra were measured with a constant acceleration spectrometer (SEE Co, Minneapolis, MN). Samples were prepared by suspending 60-100 mg of ground analyte in Paratone oil and immobilized by rapid freezing in liquid nitrogen. Isomer shifts are given relative to Fe foil at room temperature. Data were analyzed and simulated with Igor Pro 6 software (WaveMetrics, Portland, OR) using Lorentzian fitting functions.

Magnetic data were collected on a Quantum Design MPMS3 SQUID magnetometer. Samples were prepared by placing finely ground, microcrystalline powder into a polyethylene sample holder and restraining the powder with molten eicosane. Samples were transported to the instrument under an inert atmosphere and immediately loaded into the sample chamber to minimize atmospheric exposure.

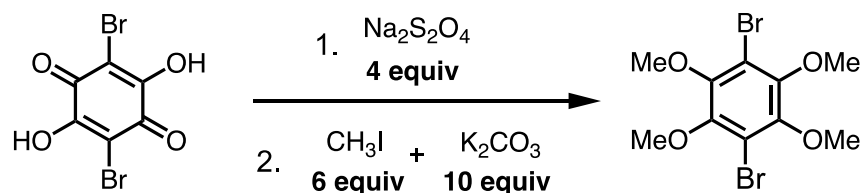
Electrical conductivity measurements were obtained using a BioLogic SP-200 Potentiostat.

2. Synthetic Procedures:

2.1 Ligand Synthesis



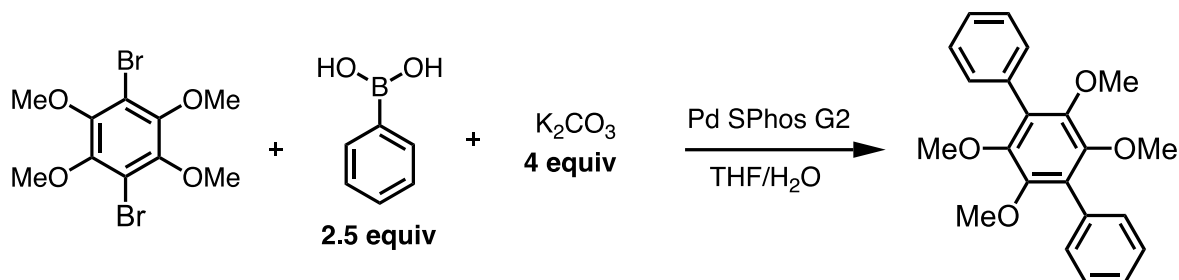
Scheme S1: General synthetic route towards Ph₂dmbq²⁻ ligands in both the reduced (H₄Ph₂dmbq) and oxidized (H₂Ph₂dmbq) forms.



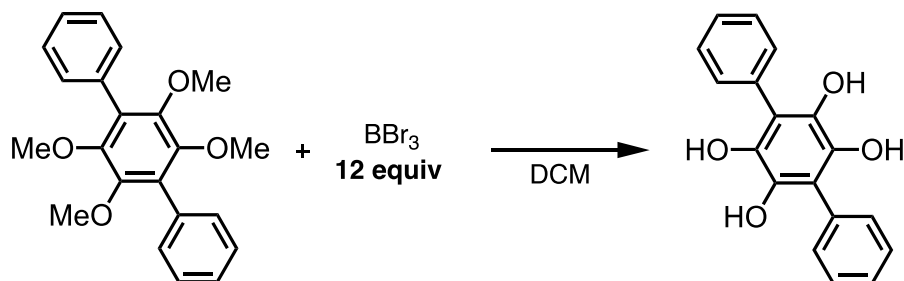
Synthesis of 1,4-dibromo-2,3,5,6-tetramethoxybenzene: This compound was prepared using modified procedures from the literature.^{1,2} A Schlenk flask was charged with bromanilic acid (2.00 g, 6.71 mmol) and EtOAc (100 mL), and the mixture was sparged with nitrogen for 30 min. While under nitrogen, a 1M aqueous sodium dithionite solution (not degassed; 26.8 mL, 26.8 mmol, 4 eq.) was added dropwise. The reaction was stirred at room temperature overnight. The EtOAc layer was isolated, and the aqueous layer was extracted with additional EtOAc (2 × 50 mL). The combined organic layers were dried over MgSO₄ and reduced to a solid *in vacuo*. The solid was suspended in DCM and filtered, washing through with additional DCM, to give 3,6-dibromobenzene-1,2,4,5-tetraol as a white solid (1.95 g, 97%). This compound was carried forward without additional characterization.

A flame-dried Schlenk flask under a nitrogen atmosphere was charged with 3,6-dibromobenzene-1,2,4,5-tetraol (3.53 g, 11.8 mmol), K₂CO₃ (16.3 g, 118 mmol, 10 eq.), and DMF (degassed/anhydrous; 70 mL). Methyl iodide (4.4 mL, 70.8 mmol, 6 eq.) was added via syringe and the mixture was stirred at room temperature overnight. The reaction was quenched with H₂O (150 mL) and stirred for 10 min. Additional H₂O (250 mL) was added to precipitate out a white

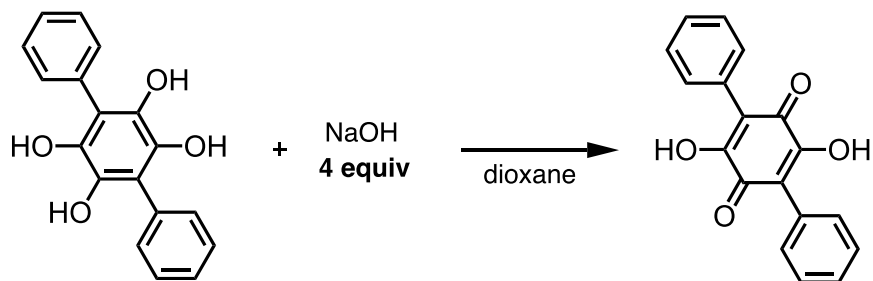
solid. The precipitate was collected by vacuum filtration and washed with H₂O (200 mL) followed by MeOH (20 mL) to yield 1,4-dibromo-2,3,5,6-tetramethoxybenzene as a white powder (3.65 g, 87%). ¹H NMR matches the previously reported spectrum for this compound.²



Synthesis of 2',3',5',6'-tetramethoxy-1,1':4,1''-terphenyl: This compound was prepared using a modified procedure from the literature.³ In a Schlenk flask, 1,4-dibromo-2,3,5,6-tetramethoxybenzene (3.51 g, 9.86 mmol), K₂CO₃ (5.45 g, 39.4 mmol, 4 eq.), and phenylboronic acid (3.00 g, 24.6 mmol, 2.5 eq.) were suspended in a mixture of THF (150 mL) and H₂O (50 mL). The mixture was sparged with nitrogen for 45 min and Pd SPhos G2 (0.142 g, 0.197 mmol, 2 mol%) was added. The reaction was refluxed under nitrogen at 70 °C for 24 hr. The THF was removed *in vacuo*, H₂O (150 mL) was added, and the solution was extracted with CHCl₃ (3 × 100 mL). The combined organic layers were washed with H₂O (100 mL), dried over MgSO₄, and the solvent was removed *in vacuo*. The resulting solid was suspended in MeOH (100 mL) and recovered via vacuum filtration before washing with additional MeOH to yield 2',3',5',6'-tetramethoxy-1,1':4,1''-terphenyl as a white, crystalline solid (3.21 g, 93%). ¹H NMR matches the previously reported spectrum for this compound.

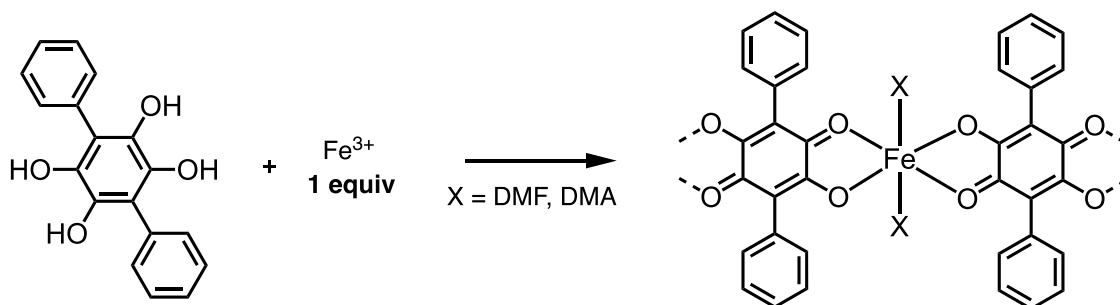


Synthesis of [1,1':4,1''-terphenyl]-2',3',5',6'-tetraol (H₄Ph₂dhbq): In an oven-dried Schlenk flask under a nitrogen atmosphere, 2',3',5',6'-tetramethoxy-1,1':4,1''-terphenyl (3.24 g, 9.25 mmol) was dissolved in DCM (degassed/anhydrous; 200 mL). The solution was cooled to -78 °C. Neat BBr₃ (10.5 mL, 111 mmol, 12 eq.) was added via cannula transfer. The cold bath was allowed to expire over the course of ~3 hr and the reaction was stirred at room temperature overnight. The reaction was cooled to 0 °C. While still under nitrogen, H₂O (not degassed; 200 mL) was added very slowly and carefully to quench the reaction. The mixture was allowed to stir for 2 hr. The cold bath was removed, and the DCM was removed *in vacuo*. The resulting precipitate was recovered by vacuum filtration. The precipitate was washed with H₂O (3 × 50 mL) followed by cold MeOH (10 mL), and allowed to dry under flowing nitrogen to yield H₄Ph₂dhbq as a white solid (2.58 g, 95%). ¹H NMR (500 MHz, MeOD): δ 6.13 (t, 6.9 Hz, 2H), 6.23 (t, 7.7 Hz, 4H), 6.29 (d, 7.2 Hz, 4H). ¹³C{¹H} NMR (75 MHz, DMSO-*d*₆ + MeOD): δ 124.27, 128.12, 129.22, 132.54, 136.27, 137.56. MS (ESI) *m/z*: 317.1 ([M+Na]⁺, calc'd for C₁₈H₁₄O₄Na: 317.1).



Synthesis of polyporic acid (H₂Ph₂dhbq): A reaction vessel was charged with H₄Ph₂dhbq (505 mg, 1.73 mmol) and *p*-dioxane (45 mL). 1M aqueous NaOH (7.0 mL, 7 mmol, 4 eq.) was added dropwise and the resulting solution was stirred open to air overnight. The reaction was acidified with 2M aqueous HCl (10 mL), diluted with H₂O (200 mL), and extracted into DCM (3 × 80 mL). The combined organic layers were washed with H₂O (80 mL) and the solvent was removed *in vacuo*. The resulting precipitate was dried under flowing N₂ to give H₂Ph₂dhbq as a brown solid (482 mg, 95%). ¹H NMR matches the previously reported spectrum for this compound.⁴

2.2 Fe(Ph₂dhbq) Chain Syntheses from Fe^{III}



Scheme S2: Generalized synthesis of *cis*-Fe(Ph₂dhbq)(DMF)₂ and *trans*-Fe(Ph₂dhbq)(DMA)₂Br_{0.55} from H₄Ph₂dhbq and Fe^{III}.

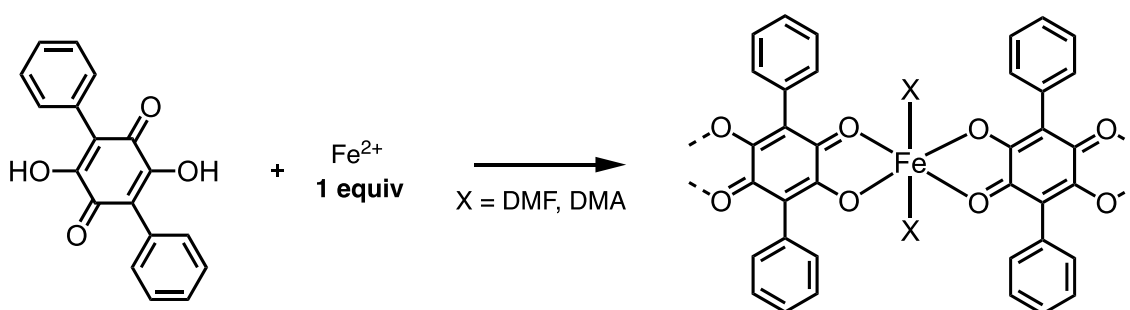
General synthesis of *cis*-Fe(Ph₂dhbq)(DMF)₂ from Fe^{III}: In a glovebox with a nitrogen atmosphere, a 20 mL scintillation vial was charged with a solution of H₄Ph₂dhbq (25.2 mg, 85.5 μmol) in 5 mL DMF. To the vial was added a solution of FeCl₃·6H₂O (23.0 mg, 85.1 μmol, 1.0 eq.) in 5 mL DMF. The vial was sealed and heated at 120 °C for 5 days to give small, dark, intergrown crystals. The mother liquor was removed, the crystals were washed with DMA (5 × 2.5 mL), and then recovered by vacuum filtration to give *cis*-Fe(Ph₂dhbq)(DMF)₂ as a dark solid (34.0 mg, 81%). Anal. Found: C, 57.57; H, 4.74; N, 5.53 (FeC₂₄H₂₄N₂O₆(H₂O)_{0.35}, calc'd: C, 57.81; H, 4.99; N, 5.62).

Synthesis of *cis*-Fe(Ph₂dhbq)(DMF)₂ from Fe^{III} for SCXRD: In a glovebox with a nitrogen atmosphere, a 4 mL scintillation vial was charged with a solution of H₄Ph₂dhbq (2.5 mg, 8.5 μmol) in 0.5 mL DMF. A solution of FeCl₃·6H₂O (2.0 mg, 7.4 μmol, 0.9 eq.) in 0.5 mL DMF was layered on top. The vial was sealed and heated at 120 °C for 1 week to give very small, dark, crystals of *cis*-Fe(Ph₂dhbq)(DMF)₂ suitable for X-ray diffraction.

General synthesis of *trans*-Fe(Ph₂dhbq)(DMA)₂Br_{0.55} from Fe^{III}: In a glovebox with a nitrogen atmosphere, a 20 mL scintillation vial was charged with a solution of H₄Ph₂dhbq (24.3 mg, 82.6 μmol) in 5 mL DMA. To the vial was added a solution of FeBr₃ (25.6 mg, 86.6 μmol, 1.0 eq.) in 5 mL DMA. The vial was sealed and heated at 120 °C for 5 days to give small, dark crystals. The mother liquor was removed, the crystals were washed with DMA (5 × 2.5 mL), and then recovered by vacuum filtration to give *trans*-Fe(Ph₂dhbq)(DMA)₂Br_{0.55} as a dark solid (15.9 mg, 37%). Anal. Found: C, 53.54; H, 5.33; N, 5.55; Br, 6.98 (FeC₂₆H₂₈N₂O₆(C₄H₉NO)_{0.40}(H₂O)_{1.05}Br_{0.55}, calc'd: C, 53.63; H, 5.49; N, 5.44; Br, 7.11).

Synthesis of *trans*-Fe(Ph₂dhbq)(DMA)₂Br_{0.55} from Fe^{III} for SCXRD: In a glovebox with a nitrogen atmosphere, a 4 mL scintillation vial was charged with a solution of H₄Ph₂dhbq (2.5 mg, 8.5 μmol) in 0.5 mL DMA. A solution of FeBr₃ (2.5 mg, 8.5 μmol, 1.0 eq.) in 0.5 mL DMA was layered on top. The vial was sealed and heated at 120 °C overnight to give small, dark crystals of *trans*-Fe(Ph₂dhbq)(DMA)₂Br_{0.55} suitable for X-ray diffraction.

2.3 Fe(Ph₂dhbq) Chain Syntheses from Fe^{II}



Scheme S3: Generalized synthesis of *cis*-Fe(Ph₂dhbq)(DMF)₂ and *trans*-Fe(Ph₂dhbq)(DMA)₂ from H₂Ph₂dhbq and Fe^{II}.

General synthesis of *cis*-Fe(Ph₂dhbq)(DMF)₂ from Fe^{II}: In a glovebox with a nitrogen atmosphere, a 20 mL scintillation vial was charged with a solution of H₂Ph₂dhbq (26.2 mg, 89.6 μmol) in 5 mL DMF. To the vial was added a solution of FeCl₂·4H₂O (16.9 mg, 84.8 μmol, 0.9 eq.) in 5 mL DMF. The vial was sealed and heated at 120 °C for 5 days to give a dark, polycrystalline powder. The solvent was removed, the powder was washed with DMF (5 × 2.5 mL), and then recovered by vacuum filtration to give *cis*-Fe(Ph₂dhbq)(DMF)₂ as a dark solid (30.3 mg, 72%). Anal. Found: C, 57.56; H, 4.88; N, 5.67 (FeC₂₄H₂₄N₂O₆(H₂O)_{0.45}, calc'd: C, 57.60; H, 5.02; N, 5.60).

General synthesis of *trans*-Fe(Ph₂dhbq)(DMA)₂ from Fe^{II}: In a glovebox with a nitrogen atmosphere, a 20 mL scintillation vial was charged with a solution of H₂Ph₂dhbq (24.9 mg, 85.1 μmol) in 5 mL DMA. To the vial was added a solution of FeCl₂·4H₂O (16.9 mg, 85.1 μmol, 1.0 eq.) in 5 mL DMA. The vial was sealed and heated at 120 °C for 5 days to give small, dark crystals. The mother liquor was removed, the crystals were washed with DMA (5 × 2.5 mL), and then recovered by vacuum filtration to give *trans*-Fe(Ph₂dhbq)(DMA)₂ as a dark solid (23.0 mg, 52%). Anal. Found: C, 59.85; H, 5.43; N, 5.49 (FeC₂₆H₂₈N₂O₆, calc'd: C, 60.01; H, 5.42; N, 5.38).

Synthesis of *trans*-Fe(Ph₂dhbq)(DMA)₂ from Fe^{II} for SCXRD: In a glovebox with a nitrogen atmosphere, a 4 mL scintillation vial was charged with a solution of H₂Ph₂dhbq (2.4 mg, 8.3 μmol) in 0.5 mL DMA. A solution of FeCl₂·4H₂O (1.7 mg, 8.6 μmol, 1.0 eq.) in 0.5 mL DMF was layered on top. The vial was sealed and heated at 120 °C for 4 days to give small, dark crystals of *trans*-Fe(Ph₂dhbq)(DMA)₂ suitable for X-ray diffraction.

3. Electrochemical Characterization:

Electrical conductivity measurements were run on pressed pellets using a home-built, two-electrode screw cell setup. A polyetheretherketone (PEEK) spacer with a 2.8 mm smooth internal diameter was prepared with threading such that two brass screws could be used to compress a powder sample from both sides. The tips of the screws were polished to a flat surface with a diameter of 2.75 mm. Cells were prepared by screwing one screw into the PEEK spacer, adding the sample, screwing in the second screw, and then tightening both screws to 0.56 Nm with a controlled torque screwdriver. All samples were removed from the glovebox and ground to a fine powder with a spatula immediately prior to analysis. 7-10 mg of sample were used per cell, and the resulting pellet thicknesses were typically in the range of 300-800 μm . After packing, the cells were allowed to settle undisturbed for 3-6 hr, before re-tightening to 0.56 Nm and allowing to settle undisturbed again overnight. Subsequently, I-V curves were collected using cyclic voltammetry between -1.0 and 1.0 V, relative to the open circuit potential, with a scan rate of 10 mV s^{-1} .

4. Dc Magnetic Measurements and Analyses:

Direct-current (dc) measurements were obtained with a 1000 G applied field and temperatures ranging from 1.8 K to 300 K. All dc measurements were corrected for the diamagnetic contribution of the sample holder, as well as the restraining material and ligand framework (calculated using Pascal's constants).⁵ Fits to the dc susceptibility were modeled using analytical solutions to the appropriate spin Hamiltonian (described below) within the Origin software package.⁶ C_{eff} was determined experimentally via linear regression of plots of $1/\chi_M$ and T (see **Figs. S15-S17**).

The dc susceptibility data of *cis*-Fe(Ph₂dhbq)(DMF)₂ were modeled using an analytical solution to the Seiden Model,⁷ derived from the following spin Hamiltonian:

$$\mathcal{H} = \sum_{i=1}^{N-1} \mathcal{H}_i, \mathcal{H}_i = J[S_i + S_{i+1}]s_i \quad (\text{S1})$$

Here, \mathbf{S}_i is the vector representation of the spin quantum number of the transition metal ions with a length of S , s_i is the spin quantum number of the radical ($S = 1/2$), and J is the metal–radical exchange coupling constant. In the low temperature limit, where J is large relative to $k_B T$, the molar susceptibility (χ_M) of the chain is described by the following expression:

$$\chi_M \cong \frac{\beta \mu_B^2 \beta J S}{3} \left(g_S S - \frac{J}{|J|} g_s s \right)^2 \quad (\text{S2})$$

Where β is $1/k_B T$, g_S and S are respectively the g factor and spin of the metal ion, and likewise g_s and s are the g factor and spin of the radical. It should be noted that this model does not account for finite chain sizes, and as such the data below the observed χT_{max} was not included in the fit. Additionally, because this model considers only metal–radical coupling, temperatures above the valence tautomerization transition temperature ($T_{1/2}$) were excluded from the fitting.

The dc susceptibility data of *trans*-Fe(Ph₂dhbq)(DMA)₂ and *trans*-Fe(Ph₂dhbq)(DMA)₂Br_{0.55} were modeled using an analytical solution derived from the classical-spin Heisenberg model for a chain of like spins (here $S = 2$ for Fe^{II}) derived from the following spin Hamiltonian:^{8,9}

$$\mathcal{H} = -2J \sum_{i=-\infty}^{+\infty} \vec{S}_i \vec{S}_{i+1} \quad (\text{S3})$$

From **Equation S3**, it has been shown that the following analytical expression can be used to describe the average susceptibility ($\langle \chi \rangle$):^{10,11}

$$\frac{\langle \chi \rangle T}{C_{\text{eff}}} \approx \frac{2}{c + 2e^{(-4\beta J S^2)}} \quad (\text{S4})$$

Here, C_{eff} is the effective Curie constant, defined as the Curie constant for a single isolated spin center in the chain, and c is the average chain length.

In order attempt to account for the presence of Robin-Day Class II/III delocalization in *trans*-Fe(Ph₂dhbq)(DMA)₂Br_{0.55}, best fits were determined by combining two, evenly weighted contributions from an extended chain of $S = 2$ ions and an extended chain of $S = 5/2$ ions. While we acknowledge this method does not truly account for the electron delocalization we observe in the Mossbauer spectra, it approximates the potential intermediacy of the oxidation states. Furthermore, the exchange coupling values did not change significantly from treating the system as entirely $S = 2$ to treating it as entirely $S = 5/2$.^{12,13}

5. Ac Magnetic Measurements and Analyses:

Alternating current (ac) magnetic susceptibility measurements were performed at zero applied magnetic field on samples made from Fe^{III} and Fe^{II}. Ac frequencies were scanned between 1 and 1500 Hz, with an oscillating field amplitude of 4 G.

The in-phase ac magnetic susceptibility (χ_M') under zero-field was modeled using an Arrhenius-like equation, which captures the temperature-dependent growth of the chain-like magnetic units from Ising spins in response to an activation energy to spin reversal:

$$\chi_M' T = C_{eff} e^{\Delta_\xi / (k_B T)} \quad (\text{S5})$$

Here, C_{eff} is the effective Curie constant, Δ_ξ / k_B is the domain wall energy, and T is the temperature. Plots of $\ln(\chi_M' T)$ versus $1/T$, ignoring the data above $T_{1/2}$ when applicable, produces a linear regime at the lowest temperatures for all samples. This enables the extraction of Δ_ξ / k_B via linear regression.

The maximum in $\chi_M' T$ also correlates to the average number of units (n) coupled via exchange (the correlation length):

$$n = (\chi_M' T_{max}) / C_{eff} \quad (\text{S6})$$

Quantitative analysis of the out-of-phase (χ_M'') susceptibility was not undertaken for several reasons. First, although out-of-phase susceptibility had non-zero signal for both the *trans*-Fe(Ph₂dhbq)(DMA)₂ and *cis*-Fe(Ph₂dhbq)(DMF)₂ samples, the relative intensity of χ_M'' to χ_M' suggests that much of the sample is not undergoing slow relaxation. In addition to the weak signal, the broadness of the observed peaks suggests that the observed relaxation phenomena are the product of more than a single relaxing species/relaxation pathway. As a result, we believe that any fitting/analysis of this data would be tenuous at best and is unlikely to provide any useful information outside of what was just discussed.

6. Single Crystal X-ray Diffraction:

Standard single-crystal X-ray diffraction (SCXRD) data was collected on a Bruker APEX II single crystal X-ray diffractometer equipped with a Mo-radiation source and a Miracol X-ray optical collimator. Synchrotron SCXRD data was collected on Beamline 12.2.1 at the Advanced Light Source (ALS), Lawrence Berkeley National Lab (Berkeley, CA, USA).

In all cases, the data was integrated and scaled using SAINT, SADABS within the APEX2 software package by Bruker.¹⁴ Solution by direct methods using SHELXT produced complete heavy atom phasing models consistent with the proposed structures.^{15,16} The structures were completed by difference Fourier synthesis with SHELXL.^{17,18} Scattering factors are from Waasmair and Kirfel.¹⁹ Hydrogen atoms were placed in geometrically idealized positions and constrained to ride on their parent atoms with C–H distances in the range 0.95–1.00 Å. Isotropic thermal parameters U_{eq} were fixed such that they were $1.2U_{eq}$ of their parent atom U_{eq} for CH's and $1.5U_{eq}$ of their parent atom U_{eq} for methyl groups. All non-hydrogen atoms were refined anisotropically by full-matrix least-squares.

SCXRD of *cis*-Fe(Ph₂dhbq)(DMF)₂ from Fe^{III} at 250 K and 100 K: A black cube, measuring $0.06 \times 0.06 \times 0.06$ mm³ was mounted on a loop with oil. Data was collected first at 250 K, then the crystal was cooled, and data was collected again at 100 K. Crystal-to-detector distance was 40 mm and exposure time was 120 seconds per frame for all sets. The scan width was 1.0°. Data collection was 100% complete to 25° in θ . A total of 4290 (250 K) or 4188 (100 K) unique reflections were collected covering the indices: $-12 \leq h \leq 12$, $-12 \leq k \leq 12$, $-22 \leq l \leq 22$. Indexing and unit cell refinement indicated a primitive trigonal (hex-setting) lattice. The space group was found to be P3₁ (No. 144). The data appeared merohedrally twinned with twin law (1 0 0, -1 -1 0, 0 0 1) which represents a twofold inversion-rotation about reciprocal coordinate (1 -1 0).

Synchrotron SCXRD of *trans*-Fe(Ph₂dhbq)(DMA)₂ at 250 K: Data was collected on a black prism, measuring $0.15 \times 0.08 \times 0.06$ mm³. Data collection was 99.9% complete to 25.93° in θ . A total of 5177 unique reflections were collected covering the indices: $-9 \leq h \leq 9$, $-15 \leq k \leq 15$, $0 \leq l \leq 16$. Indexing and unit cell refinement indicated a triclinic lattice. The space group was found to be P $\bar{1}$ (No. 2).

SCXRD of *trans*-Fe(Ph₂dhbq)(DMA)₂Br_{0.55} at 250 K: A black shard, measuring $0.25 \times 0.10 \times 0.08$ mm³ was mounted on a loop with oil. Crystal-to-detector distance was 40 mm and exposure time was 20 seconds per frame for all sets. The scan width was 0.5°. Data collection was 100% complete to 25° in θ . A total of 3780 unique reflections were collected covering the indices: $-17 \leq h \leq 17$, $-17 \leq k \leq 17$, $-7 \leq l \leq 7$, with $R_{int} = 0.1052$. Indexing and unit cell refinement indicated a primitive trigonal lattice. The space group was found to be P $\bar{3}$ (No. 147). The contribution to the diffraction pattern of disordered solvent within infinite channels along the *c*-axis was removed with SQUEEZE during structural refinement.^{20–22}

SCXRD of *trans*-Fe(Ph₂dhbq)(DMA)₂Br_{0.55} at 100 K: A black prism measuring 0.25 × 0.10 × 0.08 mm³ was mounted on a loop with oil. Crystal-to-detector distance was 40 mm and the exposure time was 30 seconds per frame for all sets. The scan width was 0.5°. Data collection was 100% complete to 25° in θ . A total of 17582 reflections were collected covering the indices: $-22 \leq h \leq 22$, $-22 \leq k \leq 22$, $-9 \leq l \leq 9$. 3030 reflections were symmetry independent with $R_{\text{int}} = 0.0841$. Indexing and unit cell refinement indicated a primitive trigonal lattice. The space group was found to be P-3 (No. 147). The contribution to the diffraction pattern of disordered solvent within infinite channels along the *c*-axis was removed with SQUEEZE.

7. Supplementary Tables:

Table S1. Select bond lengths from the single-crystal structure of *cis*-Fe(Ph₂dhbq)(DMF)₂. The C–C bond length value represents the distance between the two oxygen-bound carbon atoms within each catechol moiety.

Temp (K)	Fe–O (Å)	C–O (Å)	C–C (Å)	
250	Fe1-O1	2.08(2)	C1-O1 1.32(4)	C1-C2 1.54(6)
	Fe1-O2	2.08(3)	C2-O2 1.26(4)	C10-C11 1.49(6)
	Fe1-O3	2.13(2)	C10-O3 1.26(4)	
	Fe1-O4	2.06(2)	C11-O4 1.26(4)	
100	Fe1-O1	1.973(15)	C1-O1 1.31(3)	C1-C2 1.48(4)
	Fe1-O2	1.992(16)	C2-O2 1.29(3)	C10-C11 1.43(4)
	Fe1-O3	2.002(16)	C10-O3 1.32(3)	
	Fe1-O4	1.996(15)	C11-O4 1.30(3)	

Table S2. Select bond lengths from the single-crystal structure of *trans*-Fe(Ph₂dhbq)(DMA)₂. The C–C bond length value represents the distance between the two oxygen-bound carbon atoms within each catechol moiety.

Temp (K)	Fe–O (Å)	C–O (Å)	C–C (Å)	
250	Fe1-O1	2.1047(13)	C1-O1 1.265(2)	C1-C2 1.532(3)
	Fe1-O2	2.0850(12)	C2-O2 1.263(2)	C14-C15 1.535(3)
	Fe2-O4	2.1089(13)	C14-O4 1.261(2)	
	Fe2-O5	2.0856(12)	C15-O5 1.267(3)	

Table S3. Select bond lengths from the single-crystal structure of *trans*-Fe(Ph₂dhbq)(DMA)₂Br_{0.55}. The C–C bond length value represents the distance between the two oxygen-bound carbon atoms within each catechol moiety.

Temp (K)	Fe–O (Å)		C–O (Å)		C–C (Å)	
250	Fe1-O1	2.035(2)	C1-O2	1.279(4)	C1-C2	1.508(5)
	Fe1-O2	2.034(3)	C2-O1	1.275(4)		
100	Fe1-O1	2.019(3)	C1-O2	1.284(4)	C1-C2	1.503(5)
	Fe1-O2	2.018(3)	C2-O1	1.282(4)		

Table S4. Shortest inter- and intrachain Fe–Fe distances observed in the single-crystal structures of *cis*-Fe(Ph₂dhbq)(DMF)₂, *trans*-Fe(Ph₂dhbq)(DMA)₂, and *trans*-Fe(Ph₂dhbq)(DMA)₂Br_{0.55}.

Chain	Temp (K)	Intrachain (Å)	Interchain (Å)
<i>cis</i> -Fe(Ph ₂ dhbq)(DMF) ₂	250	7.968(3)	10.248(3)
	100	7.8043(17)	10.1118(13)
<i>trans</i> -Fe(Ph ₂ dhbq)(DMA) ₂	250	7.9614(9)	8.9003(7)
<i>trans</i> -Fe(Ph ₂ dhbq)(DMA) ₂ Br _{0.55}	250	7.8233(8)	9.1215(7)
	100	7.801(6)	9.046(3)

Table S5. Isomer shifts (δ) and quadrupole splitting ($|\Delta E_Q|$) obtained from data fits to Mössbauer spectra collected at 90, 210, and 240 K of *cis*-Fe(Ph₂dhbq)(DMF)₂ synthesized from Fe^{III}.

Temp (K)	Species (%)	δ (mm s ⁻¹)	$ \Delta E_Q $ (mm s ⁻¹)
240	100	1.12	2.48
210	55	1.18	2.50
210	45	0.55	1.46
90	100	0.64	1.30

Table S6. Isomer shifts (δ) and quadrupole splitting ($|\Delta E_Q|$) obtained from data fits to Mössbauer spectra collected at 90 and 240 K of *trans*-Fe(Ph₂dhbq)(DMA)₂.

Temp (K)	Species (%)	δ (mm s ⁻¹)	$ \Delta E_Q $ (mm s ⁻¹)
240	100	1.17	1.43
90	50	1.22	1.64
90	50	1.24	2.17

Table S7. Isomer shift (δ) and quadrupole splitting ($|\Delta E_Q|$) obtained from the data fit to the Mössbauer spectrum collected at 240 K for *trans*-Fe(Ph₂dhbq)(DMA)₂Br_{0.55}.

Temp (K)	Species (%)	δ (mm s ⁻¹)	$ \Delta E_Q $ (mm s ⁻¹)
240	100	0.79	1.59

Table S8. Linear best fit parameters for the I-V curves and derived electrical conductivity values for *cis*-Fe(Ph₂dhbq)(DMF)₂ synthesized from Fe^{III}.

Replicate	I-V Slope (Ω)	I-V Slope (R ²)	Conductivity (S cm ⁻¹)	Average (S cm ⁻¹)
1	3.2×10^7	0.9999986	2.4×10^{-8}	
2	3.7×10^7	0.9998281	2.2×10^{-8}	$2.31 \pm 0.13 \times 10^{-8}$
3	4.5×10^7	0.9999372	2.4×10^{-8}	

Table S9. Linear best fit parameters for the I-V curves and derived electrical conductivity values for *cis*-Fe(Ph₂dhbq)(DMF)₂ synthesized from Fe^{II}.

Replicate	I-V Slope (Ω)	I-V Slope (R ²)	Conductivity (S cm ⁻¹)	Average (S cm ⁻¹)
1	2.8×10^7	0.9998651	3.5×10^{-8}	
2	2.7×10^7	0.9998491	3.2×10^{-8}	$3.6 \pm 0.4 \times 10^{-8}$
3	1.5×10^7	0.9999734	4.0×10^{-8}	

Table S10. Linear best fit parameters for the I-V curves and derived electrical conductivity values for *trans*-Fe(Ph₂dhbq)(DMA)₂.

Replicate	I-V Slope (Ω)	I-V Slope (R^2)	Conductivity ($S\text{ cm}^{-1}$)	Average ($S\text{ cm}^{-1}$)
1	2.6×10^8	0.9997074	5.1×10^{-9}	
2	2.4×10^8	0.9995707	5.1×10^{-9}	$6.0 \pm 1.5 \times 10^{-9}$
3	1.1×10^8	0.9998984	7.7×10^{-9}	

Table S11. Linear best fit parameters for the I-V curves and derived electrical conductivity values for *trans*-Fe(Ph₂dhbq)(DMA)₂Br_{0.55}.

Replicate	I-V Slope (Ω)	I-V Slope (R^2)	Conductivity ($S\text{ cm}^{-1}$)	Average ($S\text{ cm}^{-1}$)
1	1.1×10^6	0.9999394	1.1×10^{-6}	
2	1.2×10^5	0.9999995	3.8×10^{-6}	$2.5 \pm 1.3 \times 10^{-6}$
3	3.2×10^5	0.9999930	2.5×10^{-6}	

Table S12. Extracted domain wall energy ($\Delta\xi/k_B$), correlation length (n), Curie constant (C_{eff}), exchange coupling (J), and g -factor (g_s) for *cis*-Fe(Ph₂dhbq)(DMF)₂, *trans*-Fe(Ph₂dhbq)(DMA)₂, and *trans*-Fe(Ph₂dhbq)(DMA)₂Br_{0.55} obtained as described above.

Chain	$\Delta\xi/k_B$ (cm^{-1})	n	C_{eff}	J (cm^{-1})	g_s
<i>cis</i> -Fe(Ph ₂ dhbq)(DMF) ₂	37.03	12	3.21	-230 (± 4)	2.38
<i>trans</i> -Fe(Ph ₂ dhbq)(DMA) ₂	6.02	4	3.70	+0.30 (± 0.05)	2.3
<i>trans</i> -Fe(Ph ₂ dhbq)(DMA) ₂ Br _{0.55}	12.19	4	4.12	+0.64 (± 0.01)	-

8. Supplementary Figures:

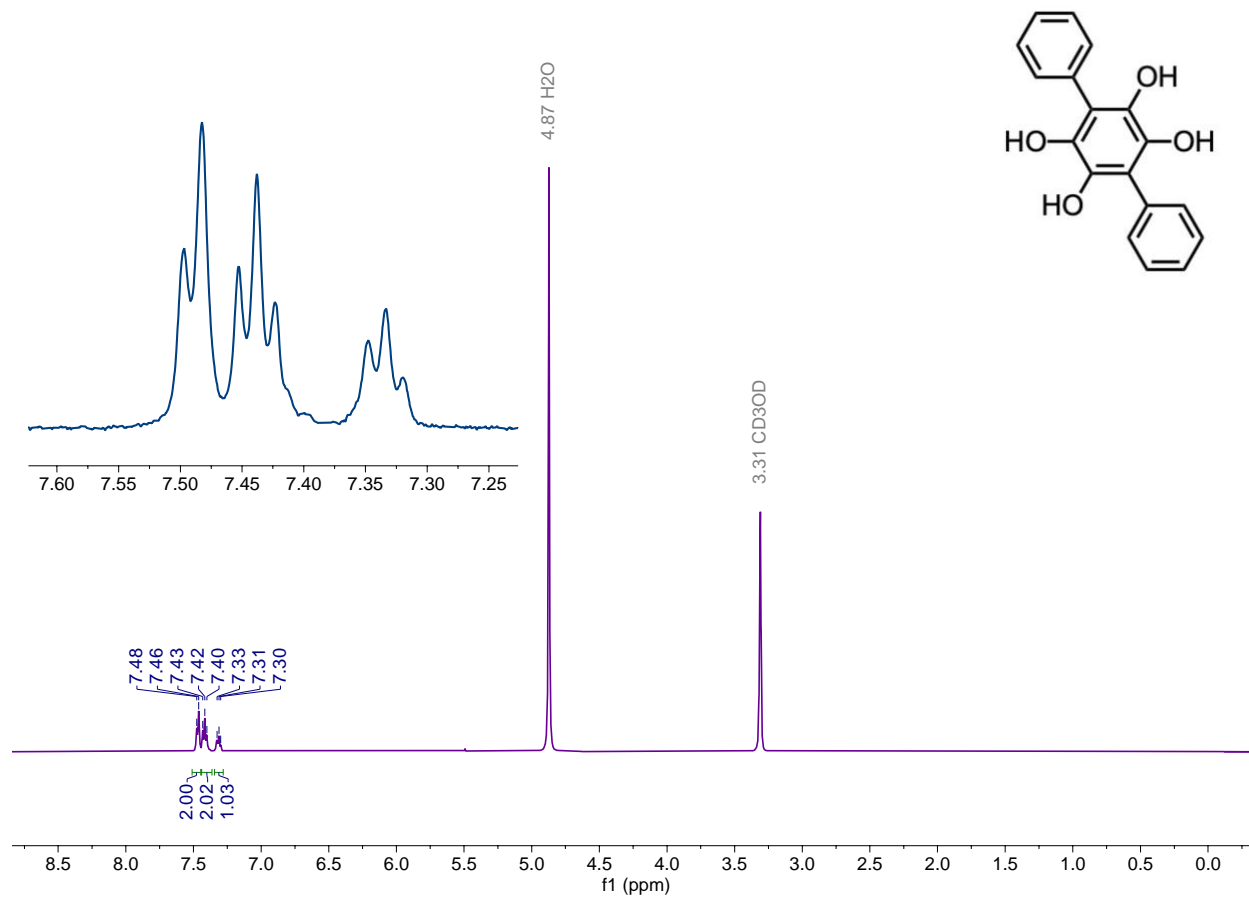


Figure S1. ¹H NMR spectrum of H₄Ph₂dwbq (500 MHz, MeOD, 298 K).

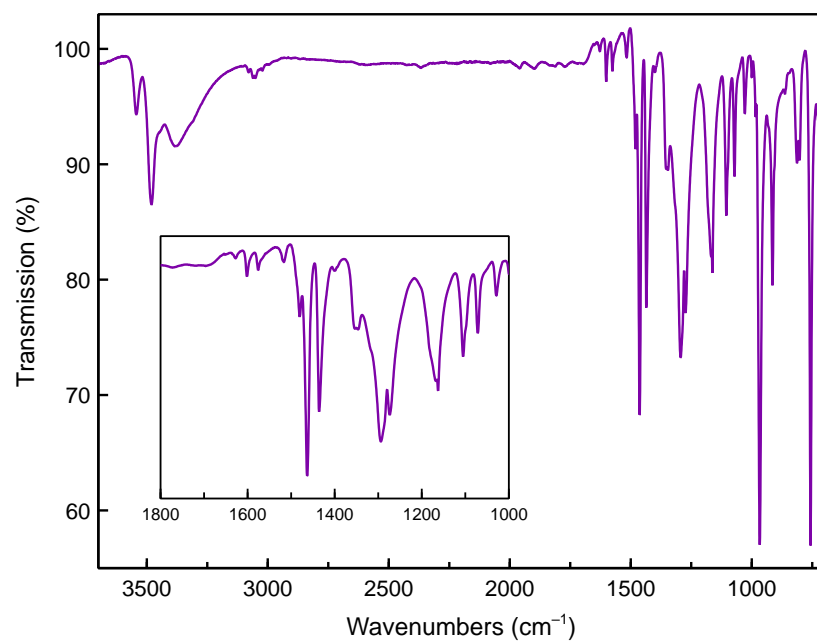


Figure S2. IR spectrum of H₄Ph₂dhbq.

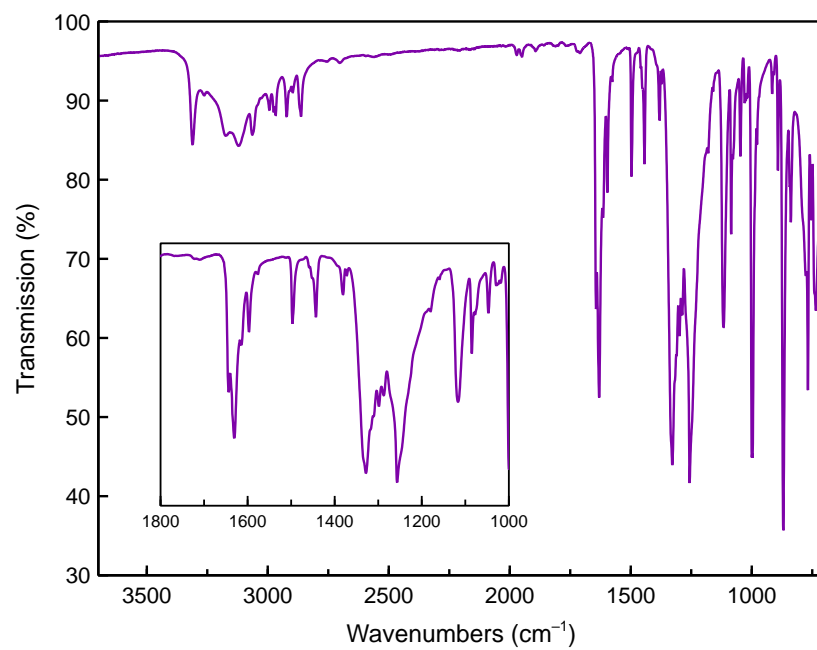


Figure S3. IR spectrum of H₂Ph₂dhbq.

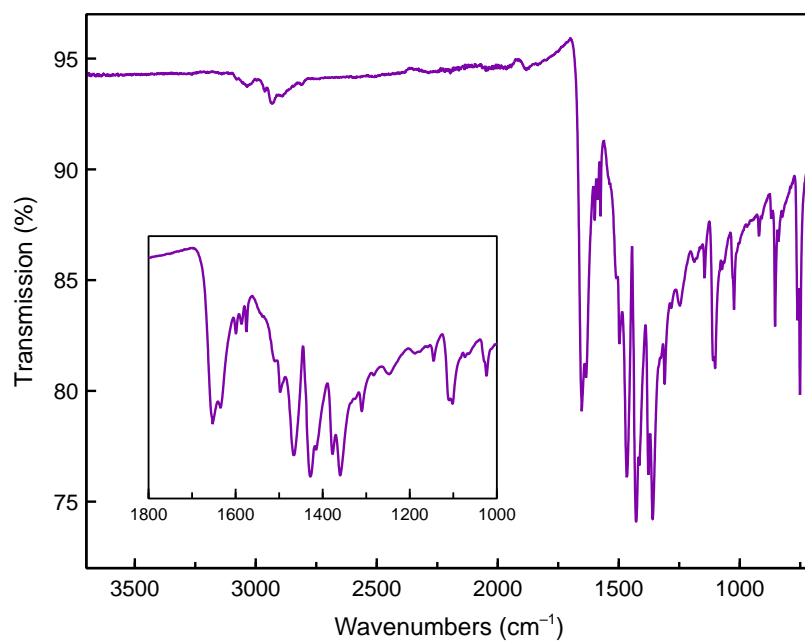


Figure S4. IR spectrum of *cis*-Fe(Ph₂dhbq)(DMF)₂ synthesized from Fe^{III}.

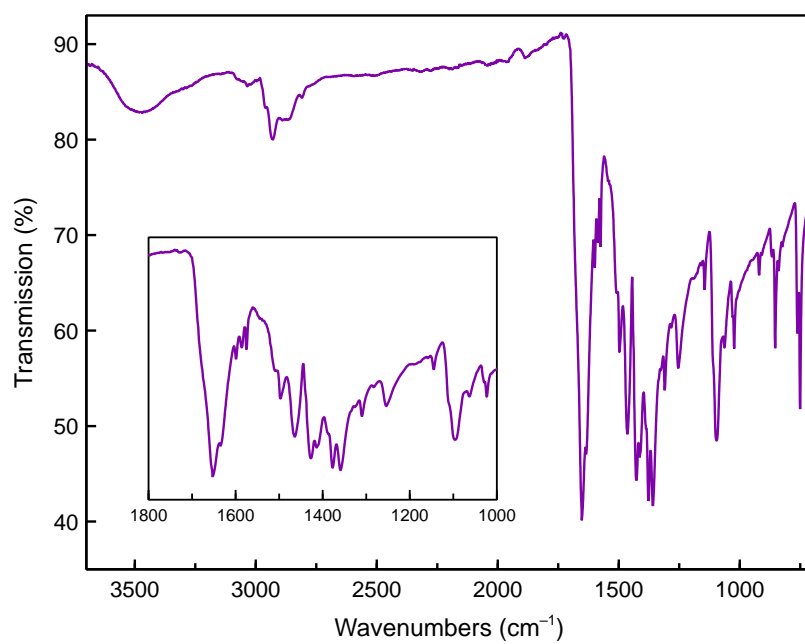


Figure S5. IR spectrum of *cis*-Fe(Ph₂dhbq)(DMF)₂ synthesized from Fe^{II}.

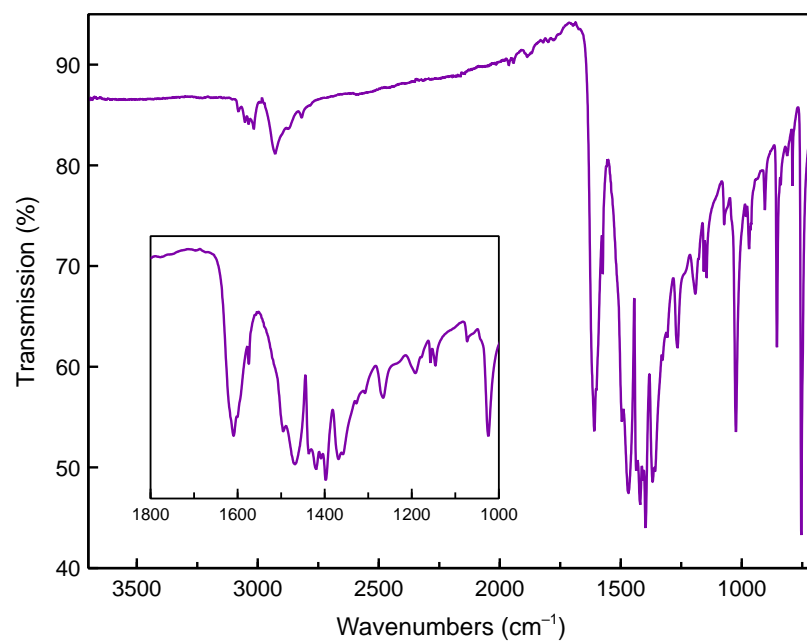


Figure S6. IR spectrum of *trans*-Fe(Ph₂dhbq)(DMA)₂.

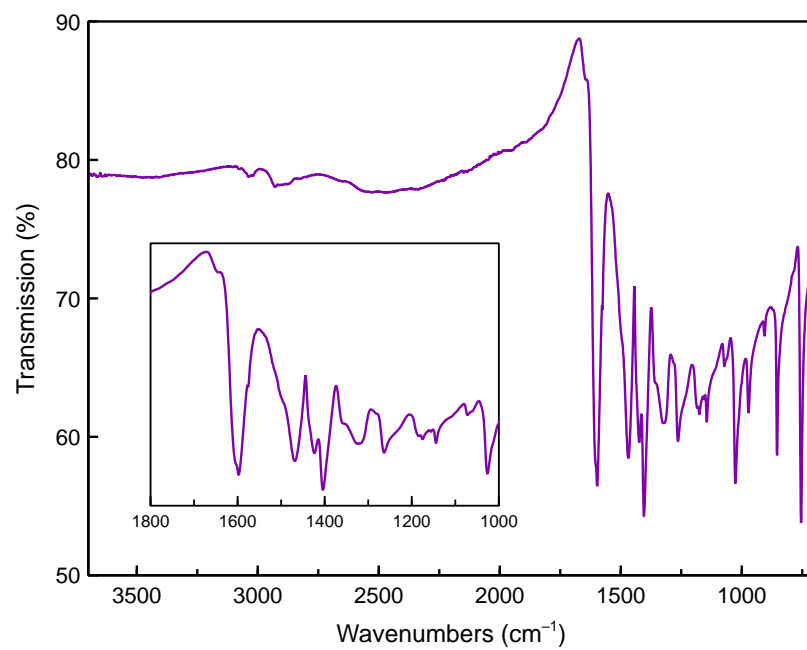


Figure S7. IR spectrum of *trans*-Fe(Ph₂dhbq)(DMA)₂Br_{0.55}.

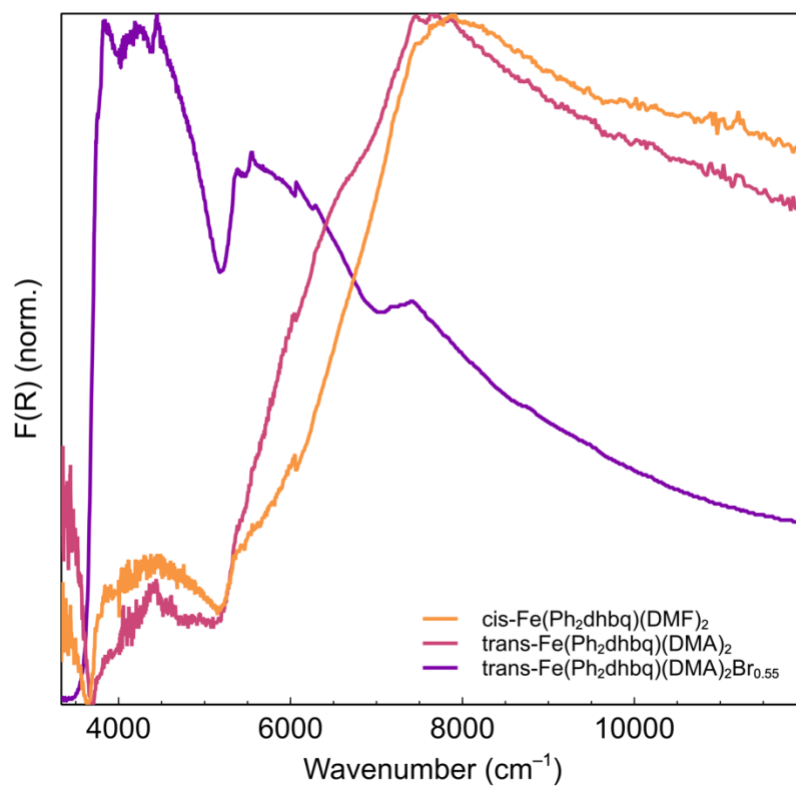


Figure S8. Normalized diffuse reflectance UV-vis-NIR spectra of *cis*-Fe(Ph₂dhbq)(DMF)₂, *trans*-Fe(Ph₂dhbq)(DMA)₂, and *trans*-Fe(Ph₂dhbq)(DMA)₂Br_{0.55}. F(R) is the Kubelka-Munk transformation of the raw reflectance data.

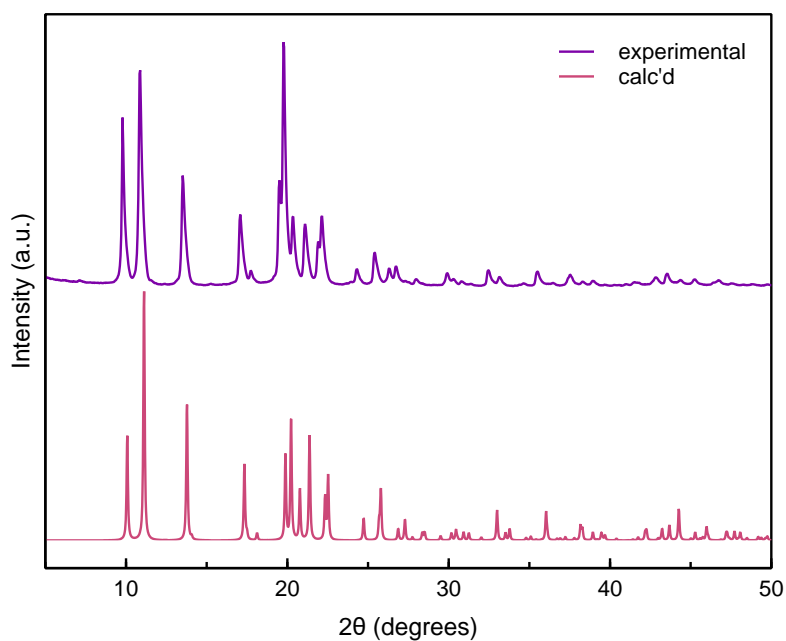


Figure S9. Experimental powder X-ray diffraction pattern of *cis*-Fe(Ph₂dhbq)(DMF)₂ synthesized from Fe^{II} versus the theoretical powder pattern calculated from the single-crystal structure of *cis*-Fe(Ph₂dhbq)(DMF)₂ synthesized from Fe^{III}. The difference in peak intensities between the experimental and theoretical powder patterns is due to preferred orientation of the crystallites on the Si substrate.

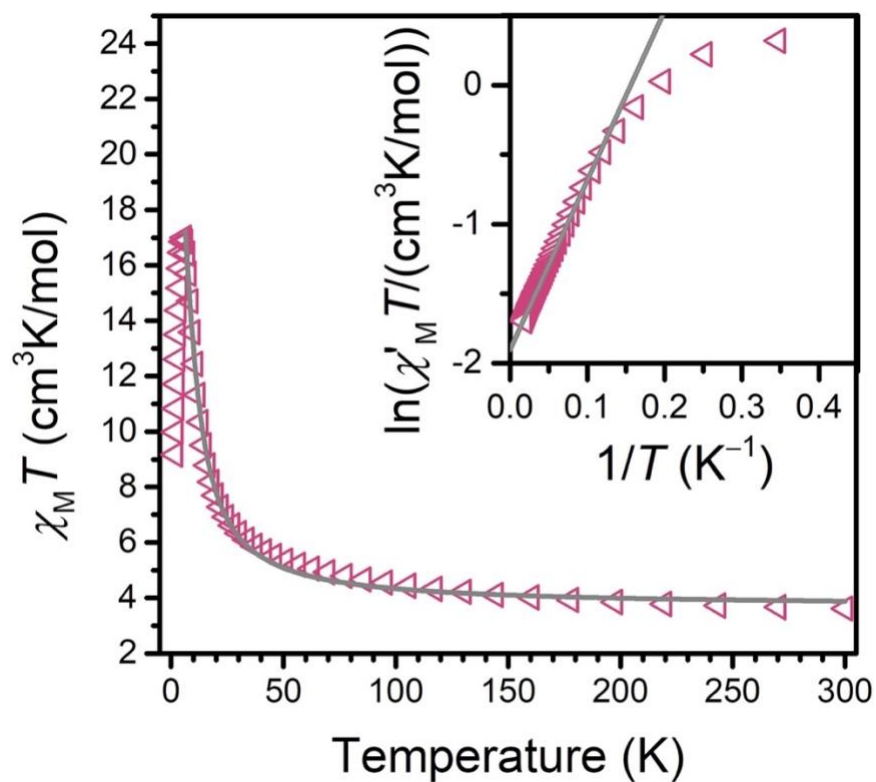


Figure S10. Dc magnetic susceptibility ($\chi_M T$) measurements for *trans*-Fe(Ph₂dhbq)(DMA)₂Br_{0.55} under an applied field of 1000 G. The solid line is a best fit with $J = +0.64 \pm 0.01 \text{ cm}^{-1}$. Inset: variable-temperature zero-field dc magnetic susceptibility (χ'_M) of *trans*-Fe(Ph₂dhbq)(DMA)₂Br_{0.55}. The gray line is a linear fit that yields a correlation length of 4. Data were collected at zero dc field with an applied ac field frequency of 1 Hz.

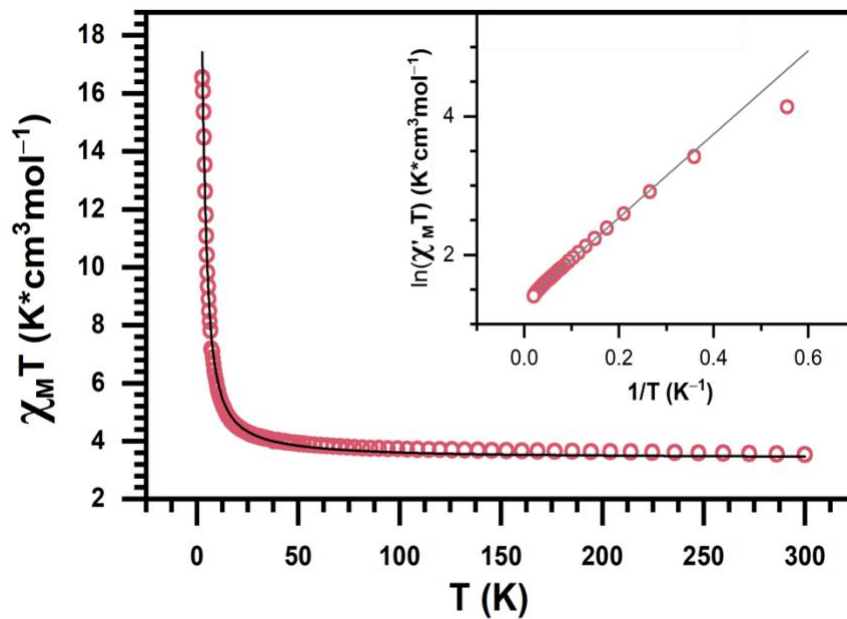


Figure S11. Dc magnetic susceptibility ($\chi_M T$) measurements for *trans*-Fe(Ph₂dmbq)(DMA)₂ under an applied field of 1000 G. The solid line is a best fit with $J = +0.30 \pm 0.05 \text{ cm}^{-1}$. Inset: variable-temperature zero-field dc magnetic susceptibility (χ'_M) of *trans*-Fe(Ph₂dmbq)(DMA)₂. The solid line is a linear fit that yields a correlation length of 4. Data were collected at zero dc field with an applied ac field frequency of 1 Hz.

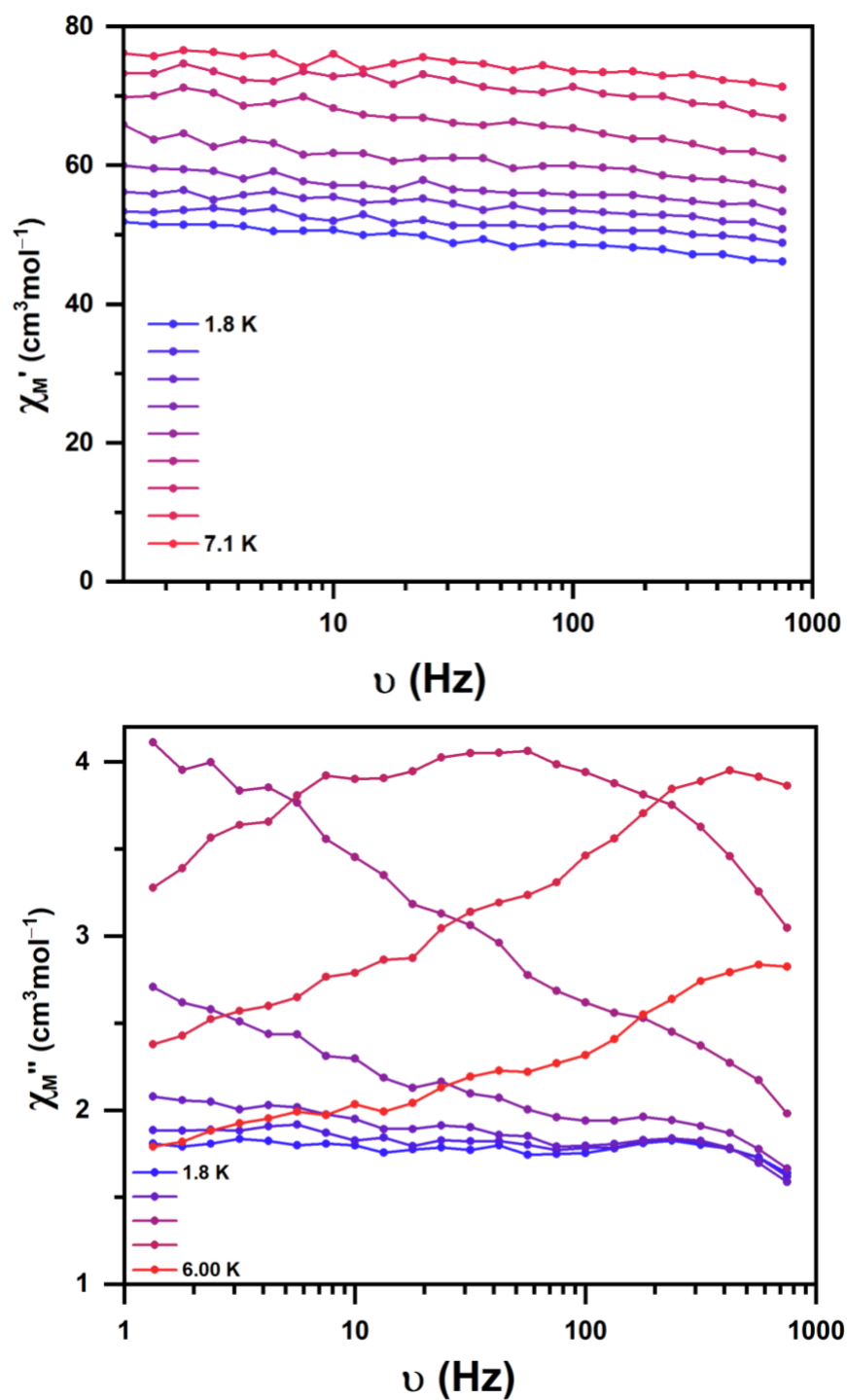


Figure S12. Frequency dependence of the in-phase (χ_M') and out-of-phase (χ_M'') ac magnetic susceptibility of ground samples of *cis*-Fe(Ph₂dhbq)(DMF)₂ synthesized from Fe^{III} at temperatures between 1.8 and 7.1 K.

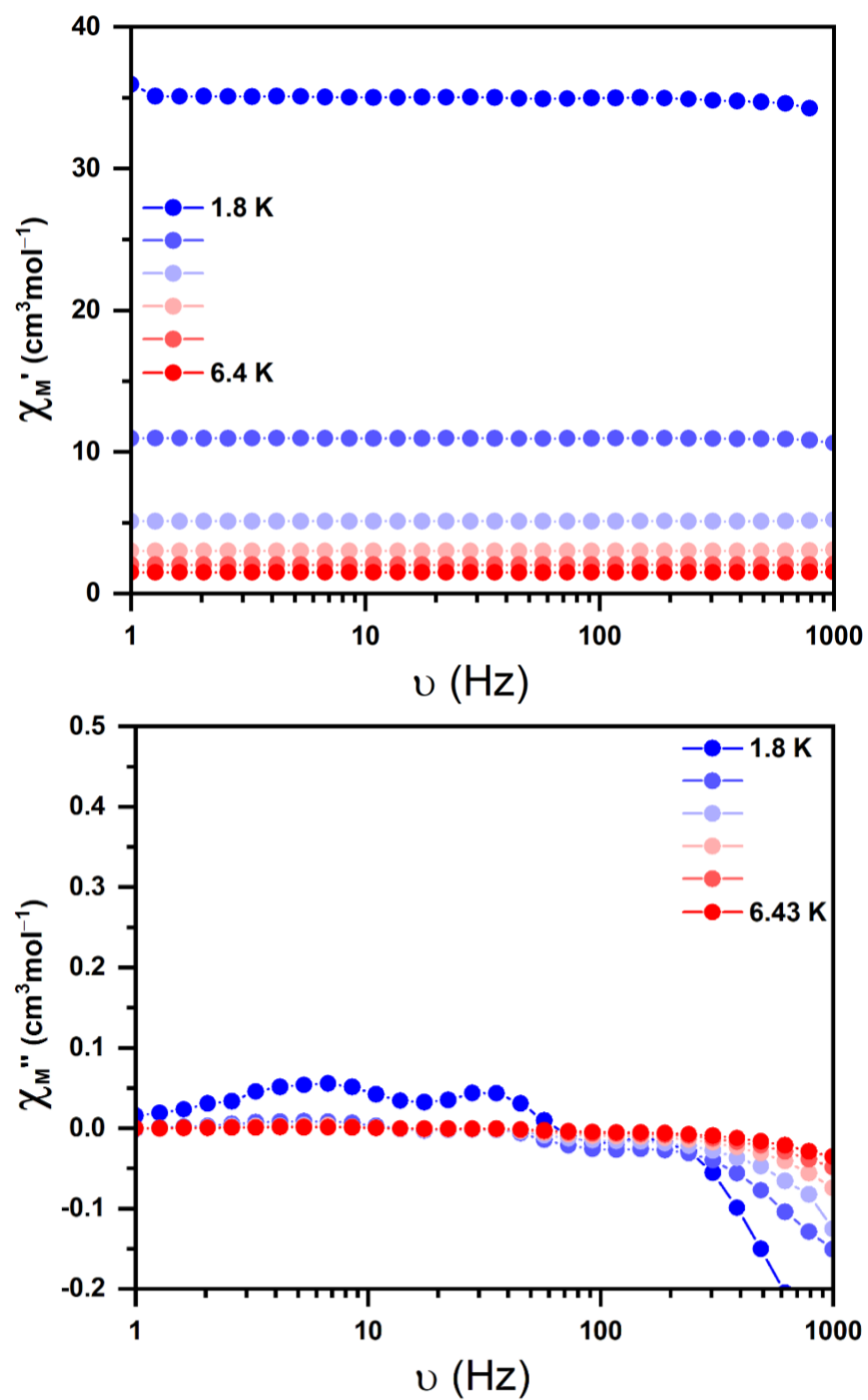


Figure S13. Frequency dependence of the in-phase (χ_M') and out-of-phase (χ_M'') ac magnetic susceptibility of ground samples of *trans*-Fe(Ph₂dhbq)(DMA)₂ at temperature between 1.8 and 6.4 K.

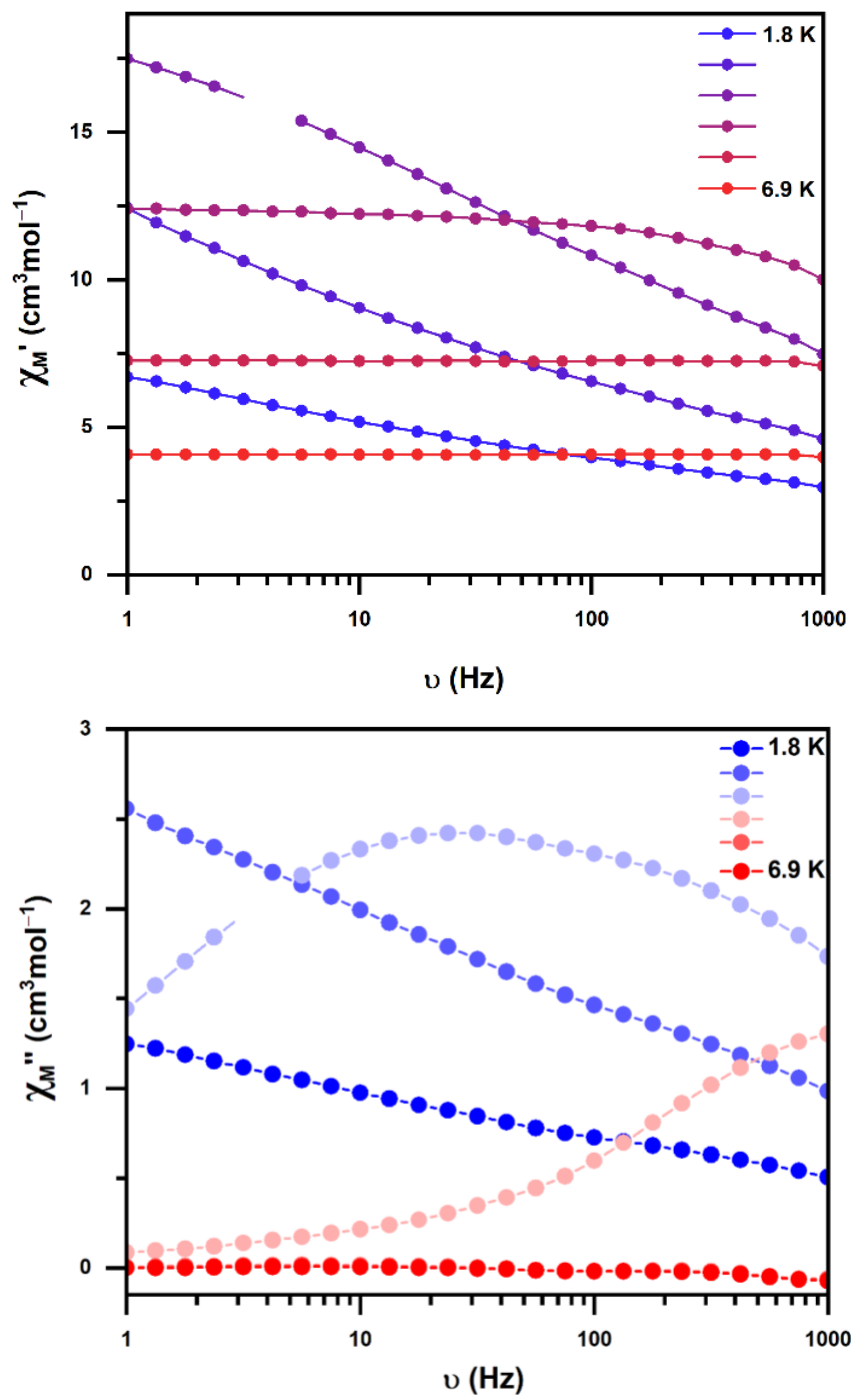


Figure S14. In-phase (χ_M') and out-of-phase (χ_M'') ac magnetic susceptibility as a function of frequency for ground samples of *trans*-Fe(Ph₂dmbq)(DMA)₂Br_{0.55} at temperatures between 1.8 and 6.9 K.

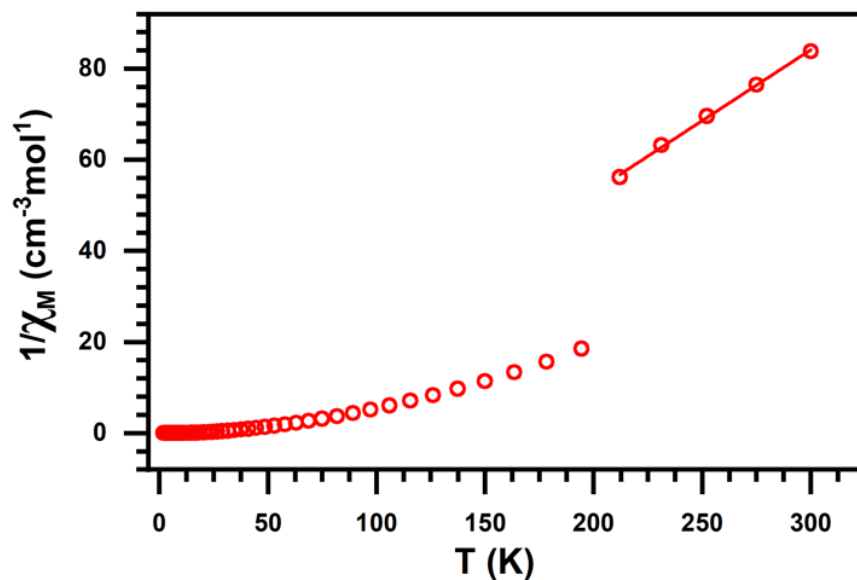


Figure S15. Inverse susceptibility as a function of temperature for *cis*-Fe(Ph₂dmbq)(DMF)₂ synthesized from Fe^{III} obtained at 1000 G. The solid line represents the linear fit used to obtain the value for C_{eff} .

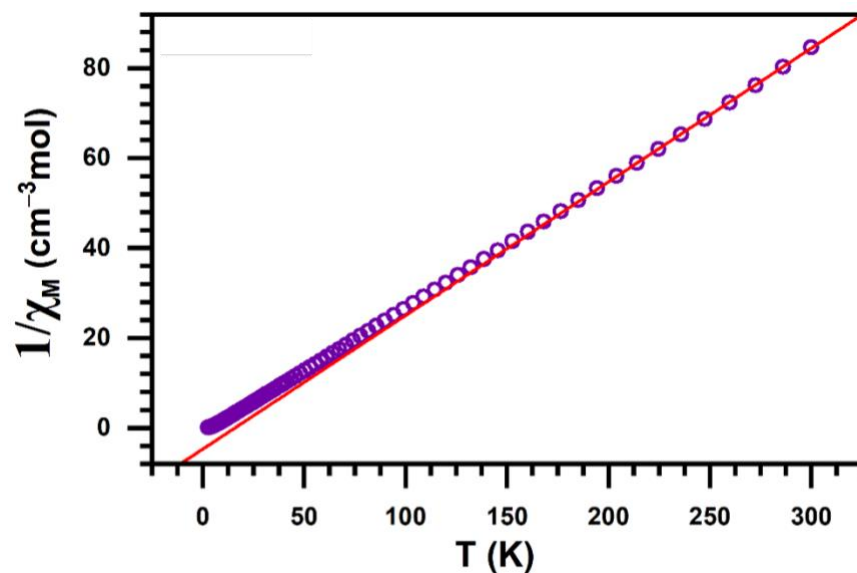


Figure S16. Inverse susceptibility as a function of temperature for *trans*-Fe(Ph₂dmbq)(DMA)₂ obtained at 1000 G. The solid line represents the linear fit used to obtain the value for C_{eff} .

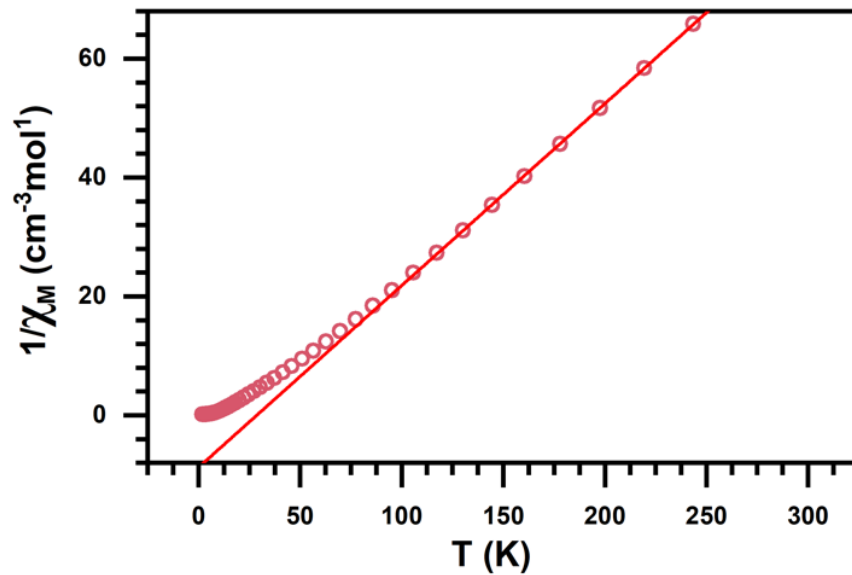


Figure S17. Inverse susceptibility as a function of temperature for *trans*-Fe(Ph₂dhbq)(DMA)₂Br_{0.55} obtained at 1000 G. The solid line represents the linear fit used to obtain the value for C_{eff} .

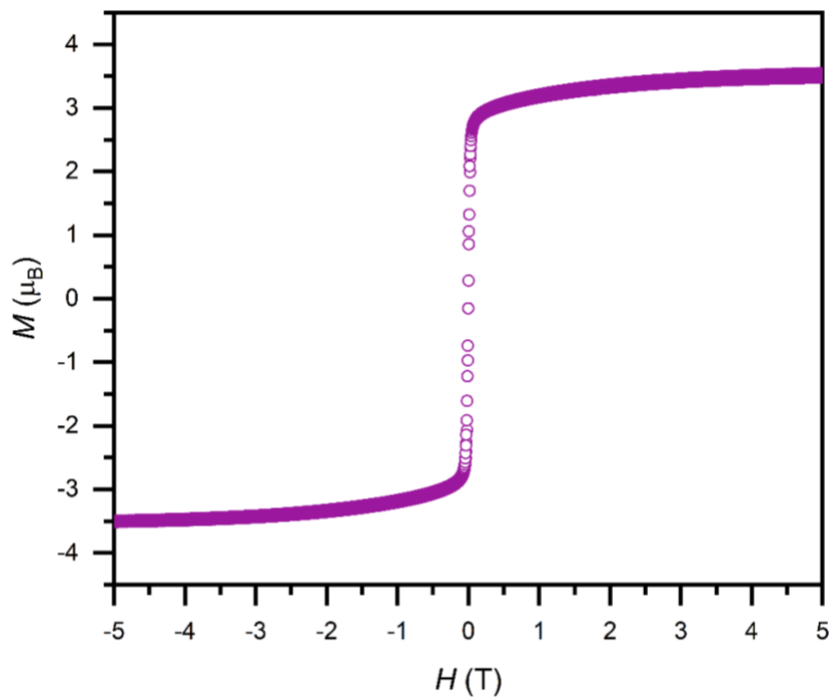


Figure S18. Variable field magnetization data for *cis*-Fe(Ph₂dhbq)(DMF)₂ collected at 2.25 K.

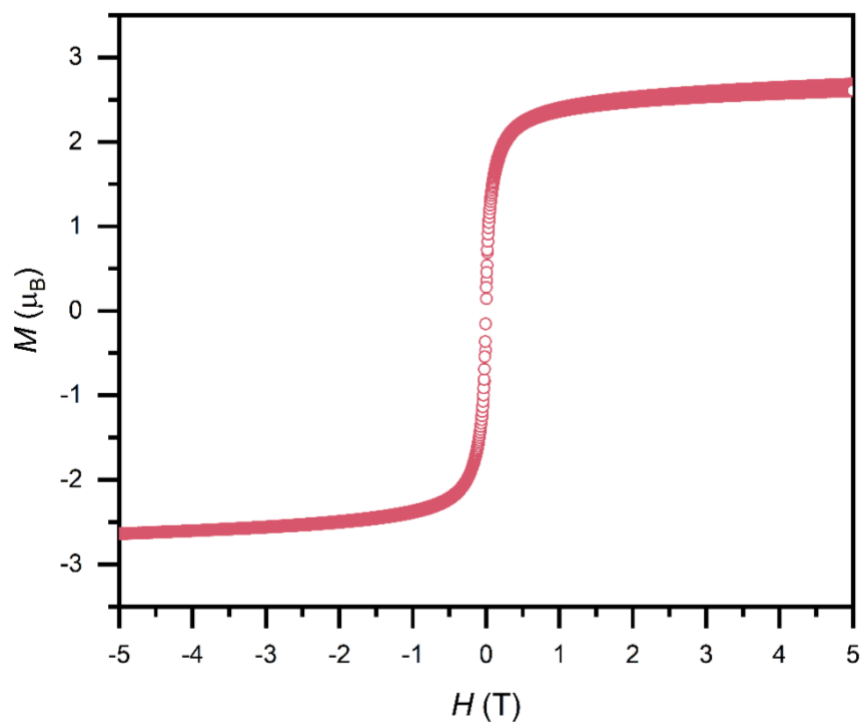


Figure S19. Variable field magnetization data for $trans\text{-Fe(Ph}_2\text{dhbq)(DMA)}_2$ collected at 2.25 K.

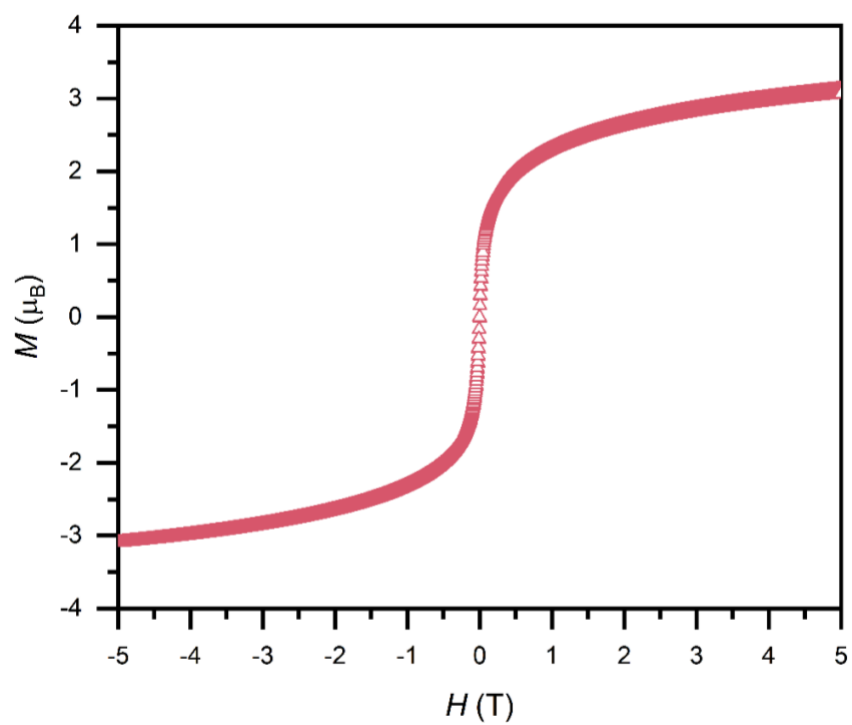


Figure S20. Variable field magnetization data for $trans\text{-Fe(Ph}_2\text{dhbq)(DMA)}_2\text{Br}_{0.55}$ collected at 2.25 K.

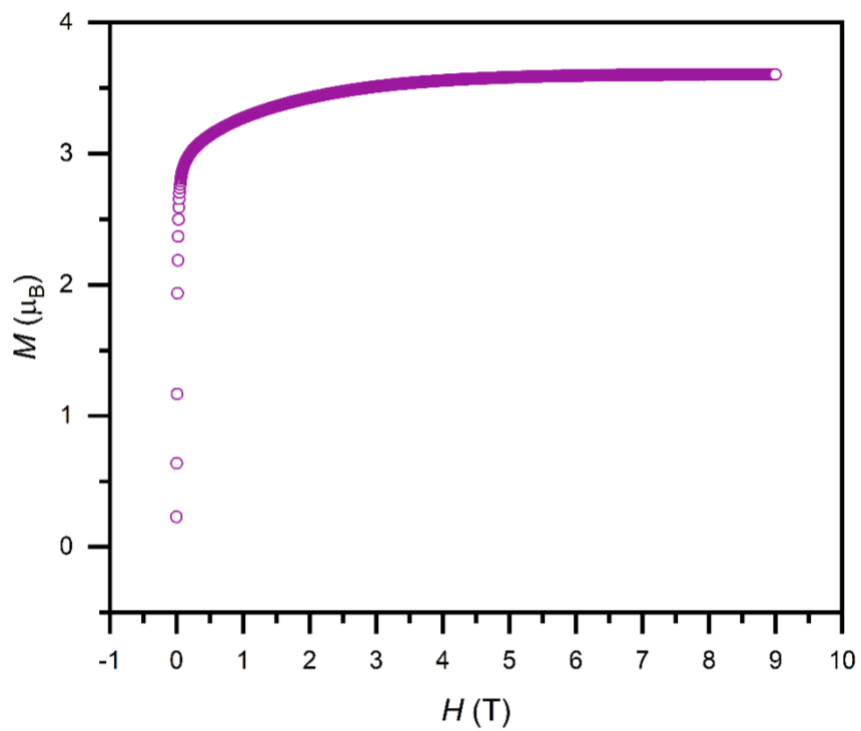


Figure S21. Variable field magnetization data for *cis*-Fe(Ph₂dhbq)(DMF)₂ collected at 2.25 K.

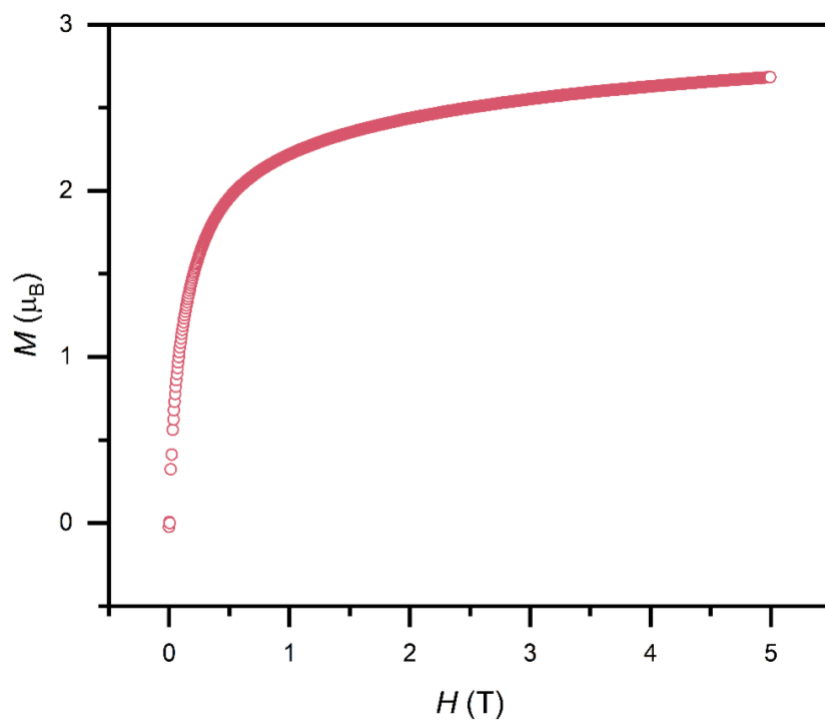


Figure S22. Variable field magnetization data for *trans*-Fe(Ph₂dhbq)(DMA)₂ collected at 2.25 K.

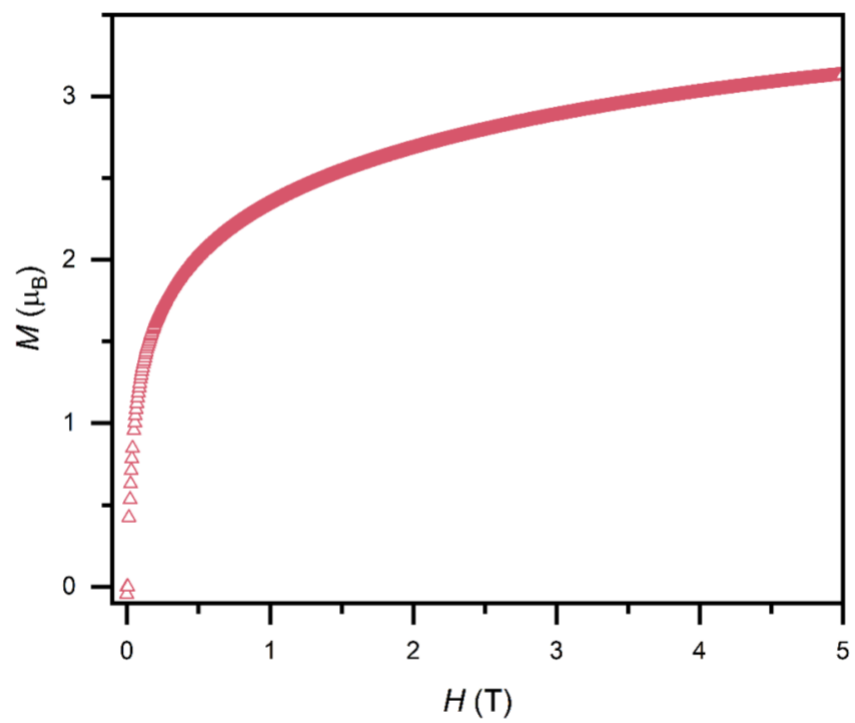


Figure S23. Variable field magnetization data for *trans*-Fe(Ph₂dhbq)(DMA)₂Br_{0.55} collected at 2.25 K.

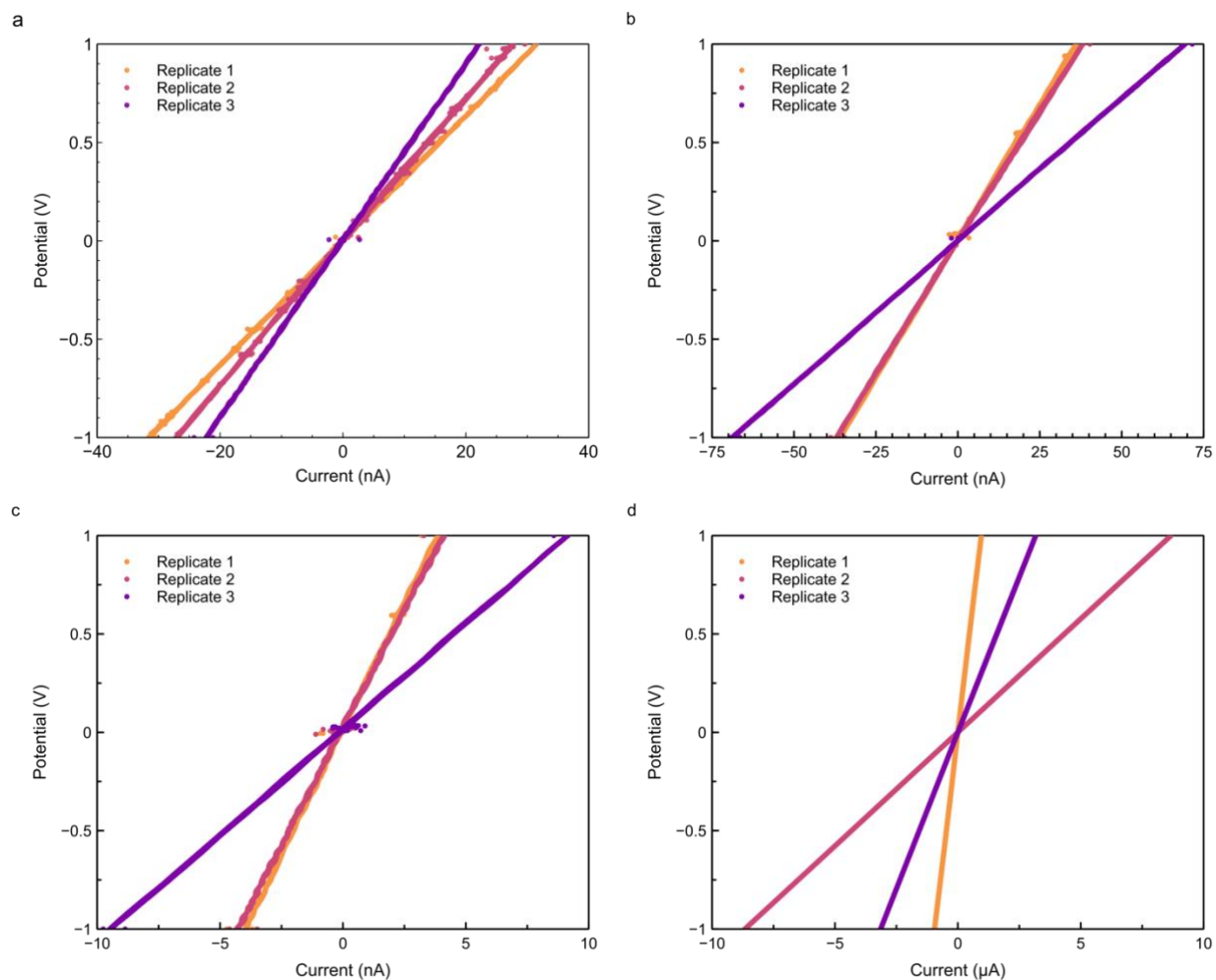


Figure S24. I-V curves used to determine the pellet electrical conductivity of (a) *cis*-Fe(Ph₂dhbq)(DMF)₂ synthesized from Fe^{III}, (b) *cis*-Fe(Ph₂dhbq)(DMF)₂ synthesized from Fe^{II}, (c) *trans*-Fe(Ph₂dhbq)(DMA)₂, and (d) *trans*-Fe(Ph₂dhbq)(DMA)₂Br_{0.55}.

9. Supplementary Crystallographic Data:

Table S13. Crystallographic parameters for the structure of *cis*-Fe(Ph₂dhbq)(DMF)₂ collected at 250 K.

Empirical formula	C ₂₄ H ₂₄ Fe N ₂ O ₆	
Formula weight	492.30	
Temperature	250(2) K	
Wavelength	0.71073 Å	
Crystal system	Trigonal	
Space group	P 3 ₁	
Unit cell dimensions	a = 10.248(2) Å	a = 90°
	b = 10.248(2) Å	b = 90°
	c = 19.033(4) Å	g = 120°
Volume	1731.0(8) Å ³	
Z	3	
Density (calculated)	1.417 Mg/m ³	
Absorption coefficient	0.696 mm ⁻¹	
F(000)	768	
Crystal size	0.060 × 0.060 × 0.060 mm ³	
Theta range for data collection	1.070 to 25.416°	
Index ranges	-12 ≤ h ≤ 12, -12 ≤ k ≤ 12, -22 ≤ l ≤ 22	
Reflections collected	4290	
Independent reflections	4260 [R _{int} = 0.1345]	
Completeness to theta = 25.000°	100.0%	
Refinement method	Full-matrix least-squares on F ²	
Data / restraints / parameters	4260 / 163 / 279	
Goodness-of-fit on F ²	1.012	
Final R indices [I > 2σ(I)]	R1 = 0.0707, wR2 = 0.1051	
R indices (all data)	R1 = 0.1867, wR2 = 0.1394	
Absolute structure parameter	0.517(6)	
Largest diff. peak and hole	0.412 and -0.434 e Å ⁻³	

Table S14. Crystallographic parameters for the structure of *cis*-Fe(Ph₂dhbq)(DMF)₂ collected at 100 K.

Empirical formula	C ₂₄ H ₂₄ Fe N ₂ O ₆	
Formula weight	492.30	
Temperature	100(2) K	
Wavelength	0.71073 Å	
Crystal system	Trigonal	
Space group	P 3 ₁	
Unit cell dimensions	a = 10.1118(12) Å	a = 90°
	b = 10.1118(12) Å	b = 90°
	c = 18.832(3) Å	g = 120°
Volume	1667.6(5) Å ³	
Z	3	
Density (calculated)	1.471 Mg/m ³	
Absorption coefficient	0.722 mm ⁻¹	
F(000)	768	
Crystal size	0.060 × 0.060 × 0.060 mm ³	
Theta range for data collection	1.081 to 25.548°	
Index ranges	-12 ≤ h ≤ 12, -12 ≤ k ≤ 12, -22 ≤ l ≤ 22	
Reflections collected	4188	
Independent reflections	4158 [R _{int} = 0.1031]	
Completeness to theta = 25.000°	100.0%	
Refinement method	Full-matrix least-squares on F ²	
Data / restraints / parameters	4158 / 163 / 279	
Goodness-of-fit on F ²	1.009	
Final R indices [I > 2σ(I)]	R1 = 0.0609, wR2 = 0.0892	
R indices (all data)	R1 = 0.1232, wR2 = 0.1075	
Absolute structure parameter	0.485(5)	
Largest diff. peak and hole	0.406 and -0.475 e Å ⁻³	

Table S15. Crystallographic parameters for the structure of *trans*-Fe(Ph₂dhbq)(DMA)₂ collected at 250 K using a synchrotron radiation source.

Empirical formula	C ₂₆ H ₂₈ Fe N ₂ O ₆	
Formula weight	520.35	
Temperature	250(2) K	
Wavelength	0.7288 Å	
Crystal system	Triclinic	
Space group	P -1	
Unit cell dimensions	a = 7.9614(8) Å	a = 90.645(4)°
	b = 12.0601(12) Å	b = 93.670(3)°
	c = 13.2291(13) Å	g = 90.906(4)°
Volume	1267.3(2) Å ³	
Z	2	
Density (calculated)	1.364 Mg/m ³	
Absorption coefficient	0.677 mm ⁻¹	
F(000)	544	
Crystal size	0.150 × 0.080 × 0.060 mm ³	
Theta range for data collection	1.582 to 27.154°	
Index ranges	-9 ≤ h ≤ 9, -15 ≤ k ≤ 15, 0 ≤ l ≤ 16	
Reflections collected/independent	5177 (merged two-component twin data)	
Completeness to theta = 25.930°	99.9%	
Refinement method	Full-matrix least-squares on F ²	
Data / restraints / parameters	5177 / 0 / 326	
Goodness-of-fit on F ²	1.057	
Final R indices [I > 2σ(I)]	R1 = 0.0326, wR2 = 0.0871	
R indices (all data)	R1 = 0.0403, wR2 = 0.0914	
Largest diff. peak and hole	0.251 and -0.294 e Å ⁻³	

Table S16. Crystallographic parameters for the structure of *trans*-Fe(Ph₂dhbq)(DMA)₂Br_{0.55} collected at 250 K.

Empirical formula	C ₂₆ H ₂₈ Fe N ₂ O ₆	
Formula weight	520.35	
Temperature	250(2) K	
Wavelength	0.71073 Å	
Crystal system	Trigonal	
Space group	P -3	
Unit cell dimensions	a = 18.2429(14) Å	a = 90°
	b = 18.2429(14) Å	b = 90°
	c = 7.8233(7) Å	g = 120°
Volume	2254.8(4) Å ³	
Z	3	
Density (calculated)	1.150 Mg/m ³	
Absorption coefficient	0.538 mm ⁻¹	
F(000)	816	
Crystal size	0.250 × 0.100 × 0.080 mm ³	
Theta range for data collection	1.289 to 28.390°	
Index ranges	-17 ≤ h ≤ 17, -17 ≤ k ≤ 17, -7 ≤ l ≤ 7	
Reflections collected	3780	
Independent reflections	3780 [R _{int} = 0.1052]	
Completeness to theta = 25.000°	100.0%	
Refinement method	Full-matrix least-squares on F ²	
Data / restraints / parameters	3780 / 0 / 210	
Goodness-of-fit on F ²	1.040	
Final R indices [I > 2σ(I)]	R1 = 0.0504, wR2 = 0.1213	
R indices (all data)	R1 = 0.0933, wR2 = 0.1384	
Largest diff. peak and hole	0.263 and -0.361 e Å ⁻³	

Table S17. Crystallographic parameters for the structure of *trans*-Fe(Ph₂dhbq)(DMA)₂Br_{0.55} collected at 100 K.

Empirical formula	C ₂₆ H ₂₈ Fe N ₂ O ₆	
Formula weight	520.35	
Temperature	100(2) K	
Wavelength	0.71073 Å	
Crystal system	Trigonal	
Space group	P -3	
Unit cell dimensions	a = 18.092(1) Å	a = 90.000(5)°
	b = 18.092(1) Å	b = 90.000(5)°
	c = 7.8010(4) Å	g = 120.000(5)°
Volume	2211.3(3) Å ³	
Z	3	
Density (calculated)	1.172 Mg/m ³	
Absorption coefficient	0.548 mm ⁻¹	
F(000)	816	
Crystal size	0.250 × 0.100 × 0.080 mm ³	
Theta range for data collection	1.300 to 26.383°	
Index ranges	-2 ≤ h ≤ 22, -22 ≤ k ≤ 22, -9 ≤ l ≤ 9	
Reflections collected	17482	
Independent reflections	3030 [R _{int} = 0.0841]	
Completeness to theta = 25.000°	100.0%	
Refinement method	Full-matrix least-squares on F ²	
Data / restraints / parameters	3030 / 0 / 210	
Goodness-of-fit on F ²	1.037	
Final R indices [I > 2σ(I)]	R1 = 0.0525, wR2 = 0.1132	
R indices (all data)	R1 = 0.0765, wR2 = 0.1232	
Largest diff. peak and hole	0.319 and -0.301 e Å ⁻³	

10. References:

- (1) Ye, Y. Q.; Koshino, H.; Onose, J.; Yoshikawa, K.; Abe, N.; Takahashi, S. First Total Synthesis of Vialinin A, a Novel and Extremely Potent Inhibitor of TNF- α Production. *Org. Lett.* **2007**, *9* (21), 4131–4134. <https://doi.org/10.1021/ol701590b>.
- (2) Tsuji, Y.; Morisaki, Y.; Chujo, Y. Construction of Aromatic-Ring-Layered Structures Using a Terphenylene-Layered Polymer as the Scaffold. *Polym. Chem.* **2013**, *4* (20), 5361–5367. <https://doi.org/10.1039/C3PY00607G>.
- (3) Morisaki, Y.; Tsuji, Y.; Chujo, Y. Synthesis of Cyclic Compounds Consisting of Face-to-Face p-Oligophenyls. *Tetrahedron Letters* **2014**, *55* (9), 1631–1634. <https://doi.org/10.1016/j.tetlet.2014.01.093>.
- (4) Clinger, J. A.; Zhang, Y.; Liu, Y.; Miller, M. D.; Hall, R. E.; Van Lanen, S. G.; Phillips Jr., G. N.; Thorson, J. S.; Elshahawi, S. I. Structure and Function of a Dual Reductase–Dehydratase Enzyme System Involved in p-Terphenyl Biosynthesis. *ACS Chem. Biol.* **2021**, *16* (12), 2816–2824. <https://doi.org/10.1021/acscchembio.1c00701>.
- (5) Bain, G. A.; Berry, J. F. Diamagnetic Corrections and Pascal’s Constants. *J. Chem. Educ.* **2008**, *85* (4), 532. <https://doi.org/10.1021/ed085p532>.
- (6) Origin (2021). OriginLab Corporation, Northampton, MA, USA.
- (7) Seiden, J. Propriétés statiques d’une chaîne isotrope alternée de spins quantiques 1/2 et de spins classiques. *J. Physique Lett.* **1983**, *44* (23), 947–952. <https://doi.org/10.1051/jphyslet:019830044023094700>.
- (8) Fisher, M. E. Magnetism in One-Dimensional Systems—The Heisenberg Model for Infinite Spin. *American Journal of Physics* **1964**, *32* (5), 343–346. <https://doi.org/10.1119/1.1970340>.
- (9) Vasiliev, A.; Volkova, O.; Zvereva, E.; Markina, M. Milestones of Low-D Quantum Magnetism. *npj Quant Mater* **2018**, *3* (1), 1–13. <https://doi.org/10.1038/s41535-018-0090-7>.
- (10) Matsubara, F.; Yoshimura, K.; Katsura, S. Magnetic Properties of One-Dimensional Dilute Ising Systems. I. *Can. J. Phys.* **1973**, *51* (10), 1053–1063. <https://doi.org/10.1139/p73-140>.
- (11) Wortis, M. Griffiths Singularities in the Randomly Dilute One-Dimensional Ising Model. *Phys. Rev. B* **1974**, *10* (11), 4665–4671. <https://doi.org/10.1103/PhysRevB.10.4665>.
- (12) *Magnetism: Molecules to Materials I: Models and Experiments*; Joel S. Miller, Marc Drillon, Eds.; Wiley-VCH Verlag GmbH & Co. KGaA, 2001.
- (13) Coulon, C.; Miyasaka, H.; Clérac, R. Single-Chain Magnets: Theoretical Approach and Experimental Systems. In *Single-Molecule Magnets and Related Phenomena*; Winpenny, R., Ed.; Structure and Bonding; Springer: Berlin, Heidelberg, 2006; pp 163–206. https://doi.org/10.1007/430_030.
- (14) Bruker (2007). APEX2 (Version 2.1-4), SAINT (Version 7.34A), SADABS (Version 2007/4). BrukerAXS Inc., Madison, Wisconsin, USA.
- (15) Sheldrick, G. M. A Short History of SHELX. *Acta Cryst A* **2008**, *64* (1), 112–122. <https://doi.org/10.1107/S0108767307043930>.
- (16) Sheldrick, G. M. SHELXT – Integrated Space-Group and Crystal-Structure Determination. *Acta Cryst A* **2015**, *71* (1), 3–8. <https://doi.org/10.1107/S2053273314026370>.
- (17) SHELDRICK, G. M. SHELXL-97, Program for the Solution of Crystal Structures. *University of Göttingen, Germany.* **1997**.

- (18) Sheldrick, G. M. Crystal Structure Refinement with SHELXL. *Acta Cryst C* **2015**, *71* (1), 3–8. <https://doi.org/10.1107/S2053229614024218>.
- (19) Waasmaier, D.; Kirfel, A. New Analytical Scattering-Factor Functions for Free Atoms and Ions. *Acta Cryst A* **1995**, *51* (3), 416–431. <https://doi.org/10.1107/S0108767394013292>.
- (20) van der Sluis, P.; Spek, A. L. BYPASS: An Effective Method for the Refinement of Crystal Structures Containing Disordered Solvent Regions. *Acta Cryst A* **1990**, *46* (3), 194–201. <https://doi.org/10.1107/S0108767389011189>.
- (21) Spek, A. L. Single-Crystal Structure Validation with the Program PLATON. *J Appl Cryst* **2003**, *36* (1), 7–13. <https://doi.org/10.1107/S0021889802022112>.
- (22) Spek, A. L. Structure Validation in Chemical Crystallography. *Acta Cryst D* **2009**, *65* (2), 148–155. <https://doi.org/10.1107/S090744490804362X>.